Cyclin A2 Induces Cytokinesis in Human Adult Cardiomyocyte and Drives Reprogramming in Mice

Esmaa Bouhamida[1], Sangeetha Vadakke-Madathil[1#], Prabhu Mathiyalagan[2#], Amaresh K. Ranjan[1,3#], Amir Khan[1], Cherrie D. Sherman[1], Paul E Miller[4], Andre Ghetti[4], Najah Abi-Gerges[4] and Hina W. Chaudhry[1*]

[1] Icahn School of Medicine at Mount Sinai, New York, NY 10029, USA
[2] Benthos Prime Central, TX, USA
[3] Pharmazz Inc., Willowbrook, IL, USA, 60527
[4] AnaBios Corporation, San Diego, CA 92109, USA
[#] Contributed equally

* Correspondence to

Hina W. Chaudhry, M.D., Department of Cardiology, Cardiovascular Regenerative Medicine, Mount Sinai School of Medicine, One Gustave L. Levy Place, Box 1030, New York, NY 10029, Phone: 212-241-4104, Fax: 212-241-5510. hina.chaudhry@mssm.edu

Abstract

Cyclin A2 (CCNA2), a master cell cycle regulator silenced in postnatal cardiomyocytes, promotes cardiac repair in animal models. However, its effect on cytokinesis in adult human cardiomyocytes remains unknown. We engineered a replication-deficient adenoviral vector encoding human CCNA2 under the cardiac Troponin T promoter and delivered it to freshly isolated cardiomyocytes from adult human hearts. Time-lapse live imaging revealed induction of complete cytokinesis with preservation of sarcomeres and calcium mobilization in redifferentiated daughter cardiomyocytes. To uncover underlying transcriptional mechanisms, single-nucleus transcriptomics of CCNA2-transgenic versus non-transgenic mouse hearts identified a cardiomyocyte subpopulation enriched for cytokinesis, proliferative, and reprogramming genes. Ultra-deep bulk RNA sequencing of adult and fetal human hearts further highlighted reprogramming pathways relevant to CCNA2-induced effects. Together, these findings demonstrate that CCNA2 can reinitiate cytokinesis in adult human cardiomyocytes and illuminate conserved molecular programs, supporting its promise as a regenerative gene therapy for the heart.

Graphical Abstract

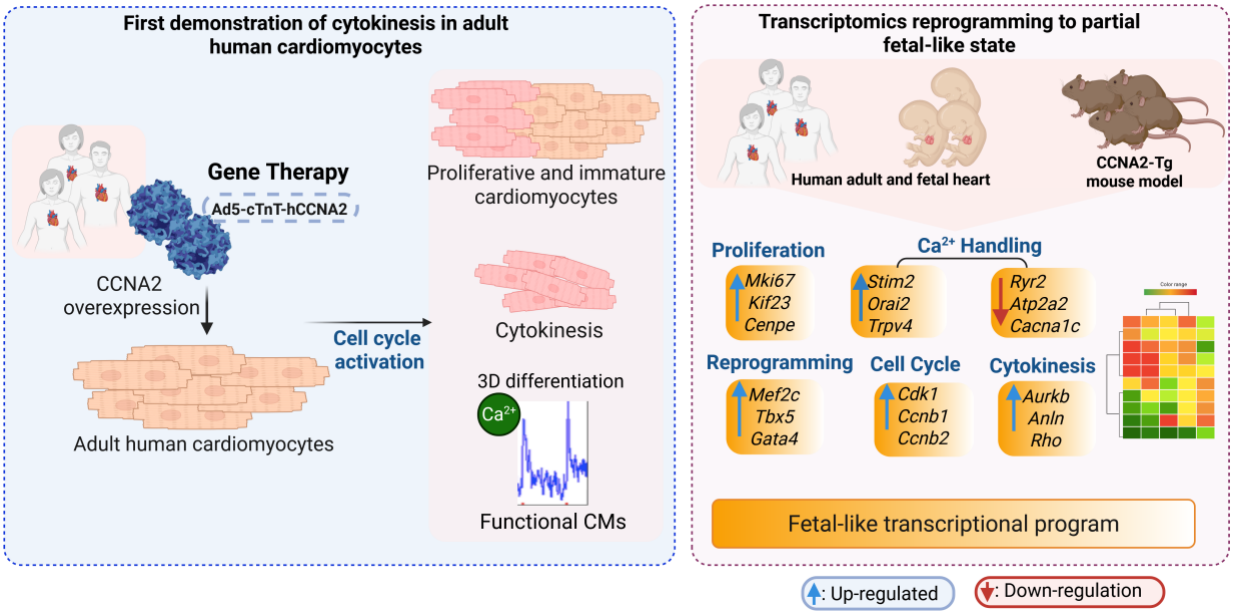

CCNA2 Induces Cytokinesis and Drives Proliferation and Reprogramming of Adult Cardiomyocytes: An Integrative Transcriptomic Analysis across Human and Mouse Models.

Introduction

The limited proliferative capacity of adult human cardiomyocytes remains a major barrier to effective cardiac regeneration following injury, contributing to the significant morbidity and mortality associated with heart disease [1]. Scar formation via fibrosis is, therefore, the primary response to cardiac injury. Multitudes of molecular and cellular approaches have been investigated over the past 20 years aimed at regenerating the myocardium in various states of heart disease [2-4]. The use of stem/progenitor cell therapies for myocardial regeneration has demonstrated limited efficacy in clinical trials, without conclusive evidence of actual cardiomyocyte differentiation arising from the cell types used previously in these trials thus far. Human embryonic stem (ES) cells and induced pluripotent (iPS) cells have been evaluated in non-human primate models of heart disease with the demonstrated ability of these cell types to differentiate, at the very least, to immature cardiomyocytes with the hope that they would undergo maturation *in vivo.* However, it remains to be seen whether these approaches may be translated for human therapy [3,5]. Beyond the differentiation and generation of new cardiomyocytes, some technical concerns still need to be addressed, such as the propensity for arrhythmias noted in primate hearts treated with ES-derived and iPS-derived cardiomyocytes [5,6].

There has been evidence of low-level cardiomyocyte turnover in the healthy human heart, but it is very limited, and this ability declines with age [7,8]. Thus, cardiac regeneration in response to injury such as myocardial infarction (MI) remains a clinical challenge. Evolution may not have favored adult mammals in this regard, but certain members of metazoan species are capable of heart regeneration, and these examples may perhaps serve to enlighten us. Urodele amphibians, such as the newt, retain a remarkable capacity to replace lost anatomical tissues through epimorphic regeneration [9]. This process relies on the local plasticity of differentiated cells near the region of injury and involves reentry to the cell cycle with loss of differentiated characteristics to generate a 'local progenitor cell' of restricted potentiality [9]. The adult zebrafish heart can regenerate up to 20% of its volume via a mechanism largely dependent on the proliferation of cardiomyocytes adjacent to the area of injury [10,11]. However, zebrafish harboring a temperature-sensitive mutation in *mps1*, a gene encoding a mitotic checkpoint kinase [10], cannot regenerate the heart, and scarring and fibrosis are noted in the excised areas in a manner similar to the response of the human myocardium after injury [10,12]. In summary, the loss of a single gene can avert cardiomyocyte mitosis and mitigate the normal regenerative process, thus permitting fibrosis to proceed unimpeded.

Previously, we have reported that CCNA2 is a 'master regulator' of the cardiomyocyte cell cycle [13]. Unlike other cyclins, cyclin A2 complexes with its cyclin-dependent kinase partners to regulate both key transitions of the cell cycle: G1-S and G2-M [14-16], and is silenced shortly after birth in mammalian cardiomyocytes [1,17,18]. Subsequently, we have also shown that *Ccna2* mediates cardiac repair by inducing cardiomyocyte mitoses after MI in two small animal models of MI [19-21]. As molecular mechanisms may be widely divergent across species, we performed a therapeutic efficacy study of CCNA2-mediated cardiac repair in a porcine model of MI as it closely mimics human anatomy and physiology [22]. Therapeutic delivery of *CCNA2* one week after MI in the porcine heart induced cardiomyocyte cell cycle activation *in vivo* with marked enhancement of

cardiac function as noted with multimodality imaging, including magnetic resonance imaging. The experimental pigs also exhibited significantly decreased fibrosis, lack of cardiomyocyte hypertrophy, and a 55% increase in cardiomyocyte cell numbers in the peri-infarct zones. Using the same viral vector encoding CCNA2 that was delivered *in vivo*, cultured porcine adult cardiomyocytes were induced to undergo cytokinesis with preservation of sarcomere structure and captured via live imaging [22].

For the purposes of clinical translation, we designed the next-generation gene therapy vector using a cardiomyocyte-specific promoter, cardiac Troponin T (cTnT), driving human CCNA2 expression in a clinical-use grade replication-deficient human adenovirus type 5. We then sought to determine whether this cTnT-CCNA2 vector would induce human adult cardiomyocytes to undergo cytokinesis. We employed a multiparametric approach combining live-cell imaging with high-resolution transcriptomics to uncover mechanistic insights underlying CCNA2-driven cytokinesis in adult cardiomyocytes. Live imaging microscopy enabled dynamic tracking of sarcomere integrity and cellular architecture during cytokinesis in adult human cardiomyocytes. To dissect the transcriptional programs and signaling pathways associated with *CCNA2* expression, we leveraged four distinct RNA sequencing datasets: (i) bulk RNA-sequencing of CCNA2-Tg and nTg cardiomyocytes, (ii) ultra-deep bulk RNA-sequencing of adult and fetal human hearts, and (iii) single-nucleus RNA sequencing (snRNA-seq, 10x Genomics). We also compared the gene expression profiles in these three datasets to previously published data regarding hypertrophic signaling pathways activated by total aortic banding (iv).

This integrative approach defined the molecular framework by which CCNA2 reactivates cell cycle networks, promotes cytokinesis, and induces a regenerative transcriptional state in postnatal cardiomyocytes, offering insights for future cardiac regenerative therapies.

Results

cTnT-CCNA2 adenovirus vector designed for therapeutic use induces expression of CCNA2 in cultured adult human cardiomyocytes

First, we designed a therapeutic grade human CCNA2 adenovirus vector to selectively express human cyclin A2 (CCNA2) in cardiomyocytes by cloning human cDNA (NCBI Reference Sequence: NM_001237.4; 374-1672 bp) downstream to the cTnT promoter **(Figure 1A)**. The cultured adult human cardiomyocytes were transduced with cTnT-hCCNA2 (test) versus cTnT-eGFP (control) adenoviruses with a multiplicity of infection (MOI) of 100 each for assessing the induced expression of CCNA2. We observed significantly increased expression of CCNA2 in the cultured adult human cardiomyocytes transduced with the test compared to the control adenovirus **(Figure 1B)**. We utilized cTnT-H2B-GFP to confirm that the nuclei of the daughter cells belonged to cardiomyocytes. A schematic overview of the study design and integrated analyses is provided in **Figure S1**.

Adenoviral vector-mediated expression of CCNA2 induces cytokinesis in cultured adult human cardiomyocytes

To assess the effect of induced CCNA2 expression on cell division in adult human cardiomyocytes, we cultured adult human cardiomyocytes and studied cytokinesis *in vitro* by using live cell epifluorescence time-lapse microscopy. The adult human cardiomyocytes were plated at equal densities and transduced with cTnT-hCCNA2, cTnT-eGFP, and/or cTnT-H2B-GFP and CMV-α-act-mCherry adenoviruses (test) or with cTnT-eGFP and/or cTnT-H2B-GFP and CMV-α-act-mCherry adenoviruses (control). cTnT-eGFP and/or cTnT-H2B-GFP adenovirus was transduced in both groups to confirm the initial tracking of cardiomyocytes (green) during live cell epifluorescence microscopy. For live visualization of sarcomeric structure in cardiomyocytes, cells from both groups were co-transduced with an adenovirus containing α-act-mCherry, which we had constructed to allow for proper folding of the virally delivered α-actinin into the live cardiomyocyte sarcomere (CMV-α-act-mCherry) and was successfully used in cultured adult porcine cardiomyocytes [22]. This strategy enabled us to confirm cardiomyocyte identity by assessing the expression of eGFP before and after cytokinesis and tracking sarcomere dynamics during live cell imaging. This approach provides a significant advantage over antibody-based identification, which is susceptible to artifacts and restricted to a single time point after cell fixation. We observed co-expression of eGFP (green) and α-actinin (red) in cultured adult cardiomyocytes **(Figure 1C** and **1H**; first panel**)**. We performed time-lapse microscopic imaging of live cells to capture cardiomyocyte cytokinesis **(Figure 1C**, **1F**, **1H,** and **Figure S2**- a still image from **movie S1)**. The cytokinetic index of adult human cardiomyocytes was calculated by counting the cytokinetic events observed in 42 regions of interest (ROIs) **(Source Data Figure 1I)**. The cytokinetic index was significantly higher in the test samples with cTnT-CCNA2 adenovirus transduction compared to control samples in the 41- and 55-year-olds **(Figure 1I)**. In contrast, no significant change in the cytokinetic events between test and control samples was observed in the 21-year-old patient's cardiomyocytes **(Figure 1I)**. Most remarkably, sarcomere structure was preserved in the daughter cells after cytokinesis **(Figure 1D** and **Figure 1G**; upon magnification of a daughter cell, the presence of sarcomeric structure is easily noted). The daughter cells were further identified with the expression of H2B-GFP (as they were originally also transduced with cTnT-eGFP and/or H2B-GFP) and noted to be mononuclear after they had been fixed and stained with DAPI **(Figure 1E** and **1H)**. Clusters of other cardiomyocytes with expression of eGFP could be seen adjacent to the daughter cells **(Figure 1E)**.

Next, we assessed the functional differentiation of cardiomyocytes by measuring the Ca^{2+} transients in CCNA2-expressing cardiomyocytes using live-cell calcium imaging under pacing conditions (0.5 Hz and 1 Hz; **Figure 2A**). Cardiomyocytes were maintained in long-term culture using a modified low-density protocol, followed by 3D embedding in agarose with low-serum, calcium-supplemented media. Ad5-cTnT-hCCNA2-transduced cardiomyocytes exhibited active, Ca^{2+} transients **(Figure 2B)**. These findings demonstrate that CCNA2 drives cytokinesis while preserving sarcomere integrity and calcium mobilization in adult human cardiomyocytes, suggesting functional re-differentiation.

CCNA2-induced transcriptional reprogramming reveals fetal gene signatures for calcium handling and sarcomere dynamics

To quantify the developmental and reprogramming landscape, we performed ultra-deep bulk RNA-sequencing of fetal (n=3) and adult (n=4) human hearts. This approach allowed us to compare the molecular signatures of CCNA2-induced cardiomyocyte reprogramming with naturally occurring fetal-like states. Our ultra-deep sequencing approach enhanced our ability to detect low-abundance transcripts, improve quantification accuracy, and provide a more comprehensive transcriptomic profile. This comparison contextualizes how CCNA2 expression modulates gene networks associated with dedifferentiation, proliferation, and calcium handling, highlighting its role in cardiac plasticity and regeneration. Notably, there were overlapping differentially expressed genes (DEGs) between adult CCNA2-Tg mouse cardiomyocytes and fetal human hearts with downregulated genes in both that were associated with cardiomyocyte maturation **(Figure 2C** and **2D)**. Furthermore, we found that calcium handling and contractility-related genes, as well as sarcomere assembly genes such as *RYR2, ATP2A2, SLC8A1, CALM1, CALM2, NEB, TTN*, and *TNNC1,* were differentially upregulated in adult human hearts compared to fetal human hearts **(Figure 2E)**.

Additionally, we performed bulk RNA-sequencing of mouse cardiomyocytes with constitutive CCNA2 expression in cardiomyocytes (CCNA-Tg mice) compared to non-Tg mice (n=6 in total). Key calcium handling genes, including *Ryr2, Atp2a2, Slc8a1,* and sarcomere assembly genes, as well as *Neb, Ttn,* and *Tnnc1,* were significantly downregulated in CCNA2-Tg cardiomyocytes. In contrast, genes involved in intracellular calcium release and store-operated calcium entry, such as *Itpr1, Orai2,* and *Stim2*, were upregulated in CCNA2-Tg mouse hearts, further aligning with the fetal gene expression profile **(Figure 2F** and **S3A-C)**. This suggests that *CCNA2* may regulate sarcomere assembly genes during cell division, thereby facilitating cardiomyocyte proliferation [23]. Furthermore, *CCNA2* appears to influence calcium mobilization post-cytokinesis, suggesting a broader role beyond cell cycle regulation, potentially impacting cardiomyocyte maturation and function.

Live-cell imaging of CCNA2-expression in adult human cardiomyocytes undergoing cytokinesis revealed that daughter cells retain sarcomeric integrity post-division. Despite RNA-sequencing data showing a significant downregulation of thin filament genes (*Neb, Tnn, Tnnc1*), structural sarcomere genes such as *Tnnt2* and *Actn2* remained stable **(Figure S3A)**, suggesting that sarcomere remodeling may occur transiently to accommodate cell division without leading to complete dedifferentiation.

Interestingly, transcriptomic profiling revealed upregulation of epithelial-to-mesenchymal (EMT) genes, including *Zeb1, Vim, Twist1,* and *Snai1*, which were highly expressed in embryonic (E10.5), early postnatal (P2) mouse hearts, downregulated in adult cardiomyocytes, and reactivated in CCNA2-Tg adult cardiomyocytes **(Figure S3D)**. In human fetal hearts, among EMT-associated genes, *ZEB1* was consistently upregulated in both human fetal and CCNA2-Tg hearts **(Figure S3E)**, supporting transient mesenchymal activation observed during neonatal heart

222 regeneration [24]. These findings suggest that CCNA2 overexpression correlates with a partial,
223 developmentally relevant mesenchymal gene program.
224
225 We next assessed whether CCNA2 reinstates pro-proliferative gene expression along the cardiac
226 developmental trajectory. Comparative bulk RNA sequencing analysis of E10.5, P2, and adult
227 CCNA2-Tg and nTg cardiomyocytes revealed consistent upregulation of canonical cell cycle
228 regulators, including *Mki67, Aurkb***,** and *Cdk1,* in CCNA2-Tg cardiomyocytes relative to adult nTg
229 controls, although their expression did not reach the embryonic and early postnatal expression
230 levels **(Figure S4A–C)**. Despite these modest fold-changes, Cohen's d effect size analysis
231 revealed moderate to large positive effects for several key proliferative genes (*Mki67, Kif23, Anln,*
232 and others) when comparing CCNA2-Tg to nTg cardiomyocytes **(Figure S4D)**, indicating that
233 CCNA2 induces biologically meaningful transcriptional reactivation of cell cycle programs. In
234 contrast, when comparing CCNA2-Tg cardiomyocytes to embryonic and early postnatal (P2),
235 Cohen's d values were negative, reflecting a high baseline proliferation in these developmental
236 periods, and indicating that CCNA2 overexpression does not fully restore fetal gene expression
237 levels. Notably, such partial reactivation of fetal and proliferative transcriptional programs can
238 have significant biological effects, as demonstrated in our prior functional studies [13,19-22].
239
240 To validate these transcriptomic findings, RT-qPCR analysis relative to early postnatal P2
241 cardiomyocytes confirmed that CCNA2-Tg adult cardiomyocytes partially re-express key cell
242 cycle and cytokinesis genes, including *Mki67, Aurka, Anln,* and *Kif23*, compared to adult nTg
243 hearts. Notably, *Ryr2* expression was reduced in both P2 and CCNA2-Tg cardiomyocytes,
244 reflecting a transcriptional shift toward a less mature state **(Figure S4E** and **S4F)**. These results
245 indicate that CCNA2 reactivates proliferation without a full reversion to fetal transcriptional
246 patterns.
247
248 Taken together, these findings suggest that the partial reprogramming induced by CCNA2 reflects
249 a controlled activation of developmental programs, consistent with regenerative responses
250 observed in neonatal hearts, and aligns with prior evidence that modest increases in cell cycle
251 gene expression can enhance cardiac regeneration capacity [13,19-22].
252

253 **Single-nucleus transcriptomic profiling reveals CCNA2-driven reprogramming in**
254 **selective cardiomyocytes, supported by integrative bulk RNA-sequencing analysis**
255
256 To investigate CCNA2-induced cardiomyocyte cytokinesis in an unbiased manner, we performed
257 snRNA-seq on hearts isolated from control non-transgenic (nTg) and *CCNA2* constitutively
258 expressing transgenic (CCNA2-Tg) adult mice (n=8 in total). Both male and female mice aged 8-
259 12 weeks were included. This approach enabled the identification of differentially expressed
260 genes across cardiac clusters in both nTg and CCNA2-Tg mice in the context of CCNA2
261 expression **(Figure 3A**, **3B)**. Notably, snRNA-seq also captured underrepresented cell types often
262 lost during enzymatic digestion in single-cell RNA-seq, thereby providing a comprehensive view
263 of cardiac cellular heterogeneity [23,25].
264

t-distributed Stochastic Neighbor Embedding (t-SNE) of combined nuclei profiles from both nTg and CCNA2-Tg mouse hearts revealed 16 major cardiac cell populations, including cardiomyocytes, endothelial cells, fibroblasts, cardiac, immune cells, and neuronal cells, distributed across 35 subclusters **(Figure 3C-E)**. Cell type clusters were annotated based on expression of canonical marker genes and validated through differential expression analysis and comparison with a publicly available reference dataset (iRhythmics FairdomHub) [26,27] **(Figure 3F** and **3G)**.

We identified several common clusters between nTg and CCNA2-Tg mice **(Figure 3E** and **Figure S6)**, with differential distribution across conditions **(Figure 3H** and **3I)**. Cardiomyocyte populations were identified by the classical marker genes (*Myh7*, *Actn2,* and *Tnnc1*) in both nTg and CCNA2-Tg hearts. Cardiomyocytes that express an enhanced level of contractility genes, including the *Ryr2*, are annotated as mature cardiomyocytes [27].

SnRNA-seq identified 11 subclusters of the ventricular cardiomyocyte (vCM) population common to both nTg and CCNA2-Tg hearts, with distinct differences in the proportion of nuclei across subclusters. Notably, the vCM1 and vCM5 were more prevalent in nTg hearts, whereas the vCM2, vCM3, vCM4, vCM6, vCM7, vCM8, vCM9, pro-vCM10, and the vCM11 were more abundant in CCNA2-Tg hearts **(Figure 3J)**.

Subclusters vCM1, vCM2, vCM4, vCM5, and vCM11 expressed cardiomyocyte maturation-related genes, particularly sarcomere development genes, calcium (Ca^{2+}) handling, and cardiac contractility genes (*Ttn*, *Pln, Ryr2*, and *Pkp2, Kcnd2*, and *Tnni3k),* regulating cardiomyogenesis and function [28]. Notably, vCM5 also expressed non-cardiac lineage markers such as *Ebf2*, implicated in brown adipocyte differentiation [29], and *Lsamp*, which guides neuronal connections [30]. In contrast, vCM3 and vCM7 showed increased expression of ATP synthase genes (*Atp5b* and *Atp5g3),* while vCM4 and vCM8 co-expressed the endothelial-associated gene vCM9 was uniquely marked by *Igfbp3*, consistent with a mid-differentiation state.

Moreover, the transcriptomic profile of the Pro-vCM10 displayed a robust cell cycle signature with high expression of early-phase proliferative genes (*Top2a, Cdc20, Cdk2d, Cdk1, Prc1, Bub1, Mki67*, and *Kif23)*, and mitotic-cytokinesis drivers (*Stmn1*) [31], alongside adhesion complex assembly and immune markers (*Cd44,* and *C1qa*) [32]. This transcriptional profile indicates an actively cycling, dedifferentiated cardiomyocyte population poised for regeneration. Remarkably, the proportion of Pro-vCM10 was significantly higher in CCNA2-Tg mouse hearts compared to nTg mouse hearts **(Figure 3J)**.

CCNA2 was expressed in cardiomyocytes, predominantly within the proliferative cluster identified in CCNA2-Tg hearts, which also expressed key cell cycle regulators **(Figure 4A** and **4B)**. This expression pattern remained consistent across the combined transcriptomic profiles of all subclusters **(Figure S7)**. The pro-vCM subcluster in CCNA2-Tg mice co-expressed proliferative markers (*Mki67* and *Kif23*) and exhibited reduced *Ryr2*, consistent with a less mature phenotype **(Figure 5A** and **5B)**. Compared to nTg cardiomyocytes, where *Ryr2* expression was higher,

308 CCNA2-Tg cardiomyocytes expressed a transcriptional signature consistent with a
309 dedifferentiated state that may facilitate cell cycle re-entry and regeneration [33].
310
311 Bulk RNA-sequencing further supported this profile, revealing coordinated downregulation of
312 sarcomere, contractility genes, and upregulation of proliferative programs in CCNA2-Tg
313 cardiomyocytes (**Figure S3A-C, Figure S4A-D**), aligning with a dedifferentiated state, which
314 facilitates cell cycle re-entry and cytokinesis. Consistently, *Ryr2* was significantly downregulated
315 in CCNA2-Tg cardiomyocytes compared to nTg controls, with expression levels approximating
316 those observed in fetal hearts **(Figure S8A** and **Figure 2E)**. This pattern was validated by the
317 quantitative PCR, where the *Ryr2* gene was downregulated in CCNA2-Tg cardiomyocytes and
318 P2 hearts compared to adult nTg cardiomyocytes **(Figure S8B)**. Together, this transcriptional
319 'immaturity' may enable the proliferative potential necessary for myocardial regeneration.
320
321 To further examine CCNA2-induced cytokinesis events, we investigated whether distinct
322 cardiomyocyte subclusters expressed genes associated with cytokinesis and/or reprogramming
323 in CCNA2-Tg mice. Intriguingly, the pro-vCM population demonstrated upregulation of core
324 cytokinesis regulators such as *Aurkb, Anln, Sept7,* and *Rho,* among others, with *Rho* and *Aurka*
325 significantly elevated in CCNA2-Tg compared to nTg mice **(Figure 5C)**. This pro-vCM subcluster
326 also showed increased expression of reprogramming genes, including *Pou5f1, Klf4, Gata4, Myc,*
327 *Sox2,* and *Tbx5*, with *Pou5f1* and *Tbx5* notably increased in CCNA2-Tg hearts compared to nTg
328 hearts **(Figure 5D)**. These findings were consistent with bulk RNA-sequencing analysis, which
329 revealed increased expression of cytokinesis- and reprogramming-associated genes in CCNA2-
330 Tg cardiomyocytes compared to nTg cardiomyocytes **(Figure S3D** and **5F)**.
331
332 Pathway enrichment analysis of CCNA2-Tg cardiomyocytes shows significant activation of cell
333 cycle, cytokinesis, and mitotic regulation pathways compared to nTg controls. Notably, Rho
334 GTPase signaling, spindle checkpoint regulation, and cytokinesis pathways were highly enriched
335 **(Figure 5E)**, indicating increased proliferation and cytoskeletal remodeling in CCNA2-Tg hearts.
336 In contrast, nTg cardiomyocytes showed enrichment in extracellular matrix organization, collagen
337 biosynthesis, and muscle contraction pathways, reflecting a more differentiated state. These
338 findings indicate that CCNA2 enhances proliferation and cellular plasticity, promoting a
339 regenerative phenotype in cardiomyocytes.
340
341 Our bulk RNA-sequencing data from mouse nTg and CCNA2-Tg cardiomyocytes yielded
342 comparable findings. We observed upregulation of *Ccnb1* and *Ccnb2* in CCNA2-Tg
343 cardiomyocytes compared to nTg cardiomyocytes, along with slight increases in the expression
344 of *Cdk1* in CCNA2-Tg cardiomyocytes **(Figure 5F)**. *Cdk1* is the sole essential cyclin-dependent
345 kinase (*CDK*), when complexed to Cyclin A2 promotes entry into mitosis, whereas Cyclin A2/Cdk2
346 is critical for the G1/S transition [13,34,35]. Key cytokinesis and proliferation genes, including *Aurka,*
347 *Aurkb, Anln, Mki67,* and *Kif23,* were upregulated in CCNA2-Tg cardiomyocytes, reinforcing the
348 role of CCNA2 in cell cycle reactivation **(Figure 5F)**. Adult human hearts exhibited downregulation
349 of proliferative and cytokinesis-related genes **(Figure 5G** and **5H)**, whereas CCNA2-Tg
350 cardiomyocytes retained a transcriptional profile favoring cell cycle progression and cytokinesis.
351

352 Moreover, we independently confirmed the transcriptional patterns observed in snRNA-seq, we
353 performed RT-qPCR for key proliferation, cytokinesis genes (*Ccna2, Mki67, Kif23, Anln, Aurka)*.
354 CCNA2-Tg cardiomyocytes exhibited elevated expression relative to nTg adults, consistent with
355 the transcriptomics data **(Figure S8C** and **S8D)**.
356
357 To further delineate CCNA2-driven transcriptional reprogramming from pathological remodeling,
358 we performed a comparative transcriptomic analysis using publicly available bulk RNA-
359 sequencing data from a mouse model of pressure overload-induced hypertrophy (TAB;
360 GSE138299). While CCNA2-Tg cardiomyocytes displayed robust induction of genes involved in
361 cell cycle progression, mitosis, cytokinesis, and mesenchymal-like programming (e.g., *Ccna2,*
362 *Ccnb2, Aurkb, Anln, Prc1, Cenpe, Mki67, Twist1, Snai1, Zeb1,* and *Vim*), hypertrophic
363 cardiomyocytes showed selective upregulation of classical hypertrophy-associated and stress-
364 response genes, including *Nppa, Myh7, Gdf15*, *Rasl11b,* and *Comp* **(Figure 5I)**, consistent with
365 previous studies [36,37]. Notably, although some cell cycle genes may be modestly increased in
366 hypertrophy, key mitotic spindle checkpoint regulators that were strongly activated in CCNA2-Tg
367 hearts remained low or unchanged in hypertrophic samples **(Figure S4G)**, suggesting that
368 hypertrophy does not fully engage the cellular machinery required for successful cell division.
369 Together, these data reinforce a key distinction between regenerative and hypertrophic responses
370 at the transcriptomic level. These transcriptomic differences are consistent with prior functional
371 studies demonstrating that CCNA2 gene therapy reduces fibrosis and improves cardiac function
372 in a large-animal myocardial infarction model without incurring an increase in cardiomyocyte size
373 [22], supporting the regenerative, rather than pathological, nature of CCNA2-induced remodeling.
374
375 Differential expression analysis further revealed that adult human hearts exhibit a greater number
376 of downregulated genes compared to the fetal heart **(Figure 5J)**, consistent with widespread
377 transcriptional silencing during cardiomyocyte maturation. In contrast, CCNA2-Tg cardiomyocytes
378 displayed a higher number of upregulated genes relative to nTg controls **(Figure S8E)**, indicating
379 broad transcriptional reactivation. This inverse pattern supports the role of *CCNA2* in restoring a
380 fetal gene expression landscape.

381 Pathway enrichment analysis of these differentially expressed genes confirmed upregulation of
382 metabolism, Ca^{2+} mobilization, and ion homeostasis pathways in adult human heart, and
383 downregulation of pathways linked to mitotic progression and developmental gene programs
384 **(Figure 5J)**. These findings support the hypothesis that CCNA2 reactivates a fetal-like
385 transcriptional program in adult cardiomyocytes, promoting cell cycle re-entry without complete
386 dedifferentiation.

387 Furthermore, pathway enrichment and gene set enrichment analysis (GSEA) revealed activation
388 of key signaling pathways associated with cardiomyocyte plasticity, proliferation, and
389 reprogramming in CCNA2-Tg cardiomyocytes. Specifically, the NOTCH signaling pathway and
390 its downstream effectors (HES/HEY) were upregulated, reinforcing CCNA2's role in progenitor-
391 like gene activation and cardiac reprogramming, in contrast to enrichment of fibrosis, cytoskeletal
392 remodeling, and calcineurin-NFAT signaling in TAB hearts, as previously described in
393 transcriptomic studies of cardiac hypertrophy [36,37]. Additionally, developmental pathways such as

TGF-beta regulation and Wnt interactions suggest a shift toward a more plastic, regenerative state. Increased signaling through MAPK, PDGF, and Jak-STAT pathways further supports enhanced proliferation and cytoskeletal remodeling. Furthermore, upregulation of focal adhesion, integrin interactions, and actin cytoskeleton regulation pathways indicate structural adaptations that facilitate cardiomyocyte dedifferentiation and division. Conversely, mitochondrial metabolism and oxidative phosphorylation, hallmarks of mature cardiomyocyte function, were significantly downregulated, aligning with a metabolic reversion to a fetal-like, proliferative phenotype in CCNA2-Tg cardiomyocytes **(Figure S8F** and **S8G)**.

In summary, our data highlight roles for *CCNA2* to enhance reprogramming and dedifferentiation, which ultimately elicits cardiomyocyte cytokinesis **(Figure 6)**. These results provide a compelling pathway forward for the clinical development of cardiac regenerative therapy based on the manipulation of CCNA2 expression in cardiomyocytes.

Discussion

Epimorphic regeneration is a conserved mechanism across evolution, allowing organ-specific repair in many metazoans, including neonatal mammals [38]. In humans, this capacity is evident in neonates, where the ventricular myocardium responds to pressure overload of congenital aortic stenosis through hyperplastic growth, whereas in older patients similar stress induces only hypertrophy. [39-41]. These clinical observations imply that the cell cycle repertoire of human neonatal cardiomyocytes is also intact, as cardiac growth is able to occur in a similar fashion to the embryonic heart.

Strategies to induce cardiomyocyte cytokinesis in adult human hearts are of critical need in order to face the growing public health crisis of congestive heart failure. To our knowledge, most cell therapy clinical trials in heart disease have provided inconsistent evidence of improvements in left ventricular ejection fraction, with a lack of evidence that the cell types utilized in patients to date actually differentiate into functional cardiomyocytes. A more direct and physiologic strategy is to reawaken proliferation within endogenous cardiomyocytes themselves. Our study provides the first demonstration that targeted expression of human CCNA2 under the control of a cardiomyocyte-specific promoter can induce complete cytokinesis in adult human cardiomyocytes, including those derived from individuals up to 55 years of age. This is a striking finding, as human cardiomyocyte turnover is thought to diminish to negligible levels by adulthood, with cytokinesis markers virtually absent beyond age 20 [7,8].

Importantly, our vector design—cTnT-driven CCNA2 delivered via clinical-grade Ad5—directly addresses two key translational barriers: (i) avoiding apoptosis or checkpoint failure that occurs with indiscriminate cell-cycle activation [42-46], and (ii) restricting CCNA2 expression to cardiomyocytes, thereby mitigating oncogenic risk in extracardiac tissues [47]. Together, these features position CCNA2 as a next-generation gene therapy platform for safe and tissue-specific cardiac regeneration.

438 Mechanistically, our findings extend beyond our prior animal studies. Human cardiomyocytes
439 isolated from 21-, 41- and 55-year-olds who had died of non-cardiac causes were cultured utilizing
440 adult mammalian cardiomyocyte culture methods developed by our laboratory [22] and modified for
441 human primary adult cardiomyocyte culture. These were then transduced with cTnT-hCCNA2.
442 Cardiomyocytes from the 41- and 55-year-olds in the experimental wells underwent complete
443 cytokinesis at a significantly higher frequency than the cardiomyocytes in the control wells. Based
444 on our previous studies of rodent cardiomyocytes, we attribute the low rate of cytokinetic events
445 we observed in the control wells to the reactivation of endogenous *CCNA2* with the prolonged
446 culture of cardiomyocytes. This is a phenomenon we have previously observed and quantified in
447 rodent cardiomyocytes, and likely not correlated with the low turnover seen in human hearts as
448 measured by 14C dating [48] as cytokinesis markers were not noted at all in human hearts over the
449 age 20 by Kühn and colleagues [7]. Similarly, the Frisén laboratory [48] used stereological and 14C
450 quantification techniques to measure cardiomyocyte exchange. They found that most
451 cardiomyocytes were never exchanged and that the substantial replacement of existing
452 cardiomyocytes was generated in the first 10 years of life, while the second decade of life focused
453 on DNA polyploidization.
454
455 It is noteworthy to mention that in the adult murine context, approximately 85–90% of
456 cardiomyocytes exist in a binucleated state [49], indicating that the nuclear count does not precisely
457 correspond to the cell count. The polyploidization of cardiomyocytes has been recognized as an
458 impediment to heart regeneration [50]. It has been reported that binucleated cardiomyocytes re-
459 entering the cell cycle are less likely to complete cytokinesis, thereby impeding the efficient
460 regeneration of cardiac tissue following injury [38]. In adult mammalian hearts, the ratio of
461 binucleated to mononucleated cardiomyocytes varies from one species to another. In rodent
462 hearts, approximately 90% are binucleated, while in human hearts, this percentage is markedly
463 lower, varying from 25-60% [51]. Thus, a greater percentage of mononuclear cardiomyocytes in the
464 human heart would enable greater efficiency of CCNA2 gene therapy to induce cardiomyocyte
465 proliferation as a repair strategy.
466
467 Our snRNA-Seq also confirms heightened cardiomyocyte plasticity of CCNA2 transgenic mice as
468 we note changes in gene expression involved in cell cycle progression and reprogramming. Ca^{2+}
469 signaling is a fundamental pathway in the regulation of cell division, cardiac contractility, and
470 remodeling [52-54]. The increase in the cytokinetic index in the test samples from 41- and 55-year-
471 olds shows the ability of *CCNA2* to stimulate intracellular Ca^{2+} mobilization. Of note, the
472 transduced cTnT-hCCNA2 (test samples) cultured cardiomyocytes isolated from a 21-year-old
473 male did not show a significant increase in cytokinetic index invoked by CCNA2 when compared
474 to the control samples, which is consistent with reports of previous investigators [7,48] that cell
475 turnover and cell division can naturally occur at younger ages in humans.
476
477 SnRNA-seq has been used to identify transcriptomic changes occurring at the single-cell level,
478 shedding light on the precise mapping of transcriptomic alterations in a cell-type-specific manner
479 in response to cellular stimulation or gene delivery [55]. Employing snRNA-seq in intact tissues
480 enables the capturing of cell-specific transcriptomics changes in a more precise manner while
481 maintaining the integrity of tissue responses, compared to isolated *in vitro* transcriptomics

482 analyses. Our strategy of using snRNA-seq is to identify cardiomyocyte-specific changes in an *in*
483 *vivo* setting in a clinically relevant CCNA2-Tg model, which allowed us to map specific changes
484 to a subpopulation of cardiomyocytes. This would not have been captured by analyzing the
485 transcriptome of isolated cardiomyocytes using bulk RNA-sequencing strategies. Live-cell
486 imaging demonstrates that CCNA2-transfected adult human cardiomyocytes successfully
487 undergo cytokinesis, with daughter cells retaining what appear to be intact sarcomeric structures.
488 However, transcriptomic analyses (bulk RNA-sequencing and snRNA-seq) revealed significant
489 downregulation of sarcomere-related genes. These findings suggest a dynamic remodeling
490 process during cytokinesis, where transcriptional downregulation of sarcomeric genes may occur
491 transiently, while structural integrity is preserved through post-transcriptional mechanisms or
492 protein stability. This highlights the intricate balance between cellular reprogramming and
493 maintenance of cardiomyocyte identity during division.
494
495 Importantly, while partial activation of fetal genes can occur in both regenerative and pathological
496 contexts, our comparative transcriptomic analysis revealed a clear divergence between CCNA2-
497 induced cardiomyocyte reprogramming and the transcriptional landscape of pressure overload-
498 induced hypertrophy. Unlike hypertrophic hearts, which are dominated by stress-responsive and
499 fibrotic gene signatures [36,37], CCNA2-Tg cardiomyocytes selectively upregulate genes involved in
500 mitosis and cytokinesis. This pattern reflects a regenerative phenotype more akin to fetal or
501 neonatal cardiomyocytes, rather than pathological remodeling. Notably, mitotic spindle
502 checkpoint regulators remain largely inactive in hypertrophic models [56]. These distinctions are
503 further supported by pathway enrichment analyses demonstrating that CCNA2 drives activation
504 of cell cycle and cytokinesis pathways, while hypertrophy engages calcineurin-NFAT signaling
505 and cytoskeletal remodeling. Together, these findings support the idea that CCNA2 expression
506 promotes a transcriptional program that is distinct from—and mechanistically incompatible with—
507 pathological hypertrophy, further highlighting its potential as a regenerative therapeutic strategy.
508 The combined molecular and functional evidence supports that CCNA2 expression drives a
509 regenerative program distinct from pathological remodeling, underscoring its promise as a
510 therapeutic strategy for myocardial repair.
511
512 Furthermore, the genes induced in the CCNA2-Tg model appear to represent a common
513 mechanism underlying cytokinesis in both male and female mice, consistent with observations in
514 human male and female hearts. Given that we identified a subset of cardiomyocytes that are
515 reprogrammed into a more proliferative state, we can envision targeting this subset in future
516 regenerative strategies. Unlike other regenerative approaches that separately target
517 cardiomyocyte proliferation or reprogramming, our findings suggest that *CCNA2* integrates both
518 processes, making it a unique therapeutic candidate for cardiac regeneration. Defining the
519 transcriptomic state of cyclin A2-expressing cardiomyocytes and their proliferative potential in
520 greater detail can enable us to recapitulate such proliferative cardiomyocytes both *in vitro* and *in*
521 *vivo* to determine whether targeting these specific subpopulations holds greater therapeutic
522 potential than targeting the entire cardiomyocyte population. The use of computational resources
523 can aid our comprehension of these molecular mechanisms for more precision-guided
524 regenerative strategies for human heart disease.
525

Another novel insight from our study is the observation that CCNA2 induces a plastic, mesenchymal-like state including upregulation of *Zeb1*, echoing mechanisms of neonatal regeneration. This transient plasticity appears to facilitate division while preserving structural integrity—a balance rarely achieved in regenerative interventions.

While these findings are promising, several limitations warrant consideration. Freshly isolated adult human cardiomyocytes, though an ideal model, are prone to culture-related cell death and variable adherence, complicating cytokinesis studies. More rapid isolation from cadaveric hearts and improved culture methods may enhance consistency. Adenoviral vectors, though used safely in clinical gene therapies, raise concerns about immunogenicity, and we are investigating alternative delivery approaches. Additionally, in vitro systems cannot fully recapitulate the in vivo cardiac environment. Our current reliance on high-resolution epifluorescence microscopy could be complemented by quantitative sarcomere scoring or super-resolution imaging to strengthen evidence of sarcomere preservation. Despite these limitations, this study represents a critical translational step, building on our prior demonstration that CCNA2 gene therapy significantly expanded cardiomyocyte numbers in porcine hearts with functional recovery, and highlights the therapeutic potential of CCNA2-induced cytokinesis in adult human cardiomyocytes.

Taken together, our results position CCNA2 as a unique therapeutic candidate that unifies cell-cycle reentry, reprogramming, and functional preservation of adult human cardiomyocytes. Unlike cell transplantation or non-specific mitogens, CCNA2 integrates proliferative drive with lineage fidelity, thereby offering a safer and more effective strategy for cardiac regeneration. Future work defining the molecular signatures of proliferative CCNA2-positive cardiomyocytes will enable the development of precision-guided therapies, whether by direct gene transfer or by reactivation of endogenous CCNA2 through antisense approaches.

By demonstrating that even middle-aged adult human cardiomyocytes can be induced to undergo complete cytokinesis, our study challenges the long-standing concept of irreversible cardiomyocyte cell-cycle exit and lays the foundation for clinically translatable, cardiomyocyte-specific regenerative therapy for heart disease.

Methods

Culture of adult human cardiomyocytes and *in vitro* cytokinesis study

Cardiomyocytes from adult human (21-year-old male, 41-year-old female, and 55-year-old male) heart tissue were isolated after enzymatic digestion at Anabios, San Diego, CA, and were shipped to our laboratory within 24 hours of isolation. Adult human cardiomyocytes were cultured according to our previously published adult porcine cardiomyocyte culture technique [22] with slight modifications. In brief, upon arrival, cells were washed with serum-free Dulbecco's modified Eagle's medium (DMEM) (Gibco, USA) twice, and 10^5 cells were seeded in 100mm untreated polystyrene plates (Corning, USA). Non-adherent cells were collected every 24 hours and centrifuged at 20xg for 2 min at room temperature. Cell pellet was washed with serum-free DMEM

569 and seeded on new polystyrene plates in modified Cardiomyocyte Culture Media (mod CMC) [22]
570 formulated by adding 13% fetal bovine serum (FBS), 2.5% horse serum, 1X nonessential amino
571 acid, 1mM sodium pyruvate, penicillin (100 U/ml), streptomycin (100 mg/ml), and fungizone (0.5
572 mg/ml) to DMEM/F12 (50:50). Cells were washed every day with serum-free DMEM, re-seeded
573 in new polystyrene plates and cultured for 3 days. On day 4, they were seeded in glass-bottom
574 24-well tissue culture plates for 20 days, with the medium changed every 4th day. The wells with
575 cardiomyocytes exhibiting adhesion and spreading were selected. Cells in these wells were
576 trypsinized and counted, and 10^3 cells per well were seeded in new glass-bottom tissue culture
577 plates. After 2 days of culture, cells were divided into two groups (test and control) and were
578 transduced with adenoviruses. The test group was transduced with cTnT-hCCNA2 along with
579 cTnT-eGFP and/or cTnT-H2B-GFP and CMV-α-act-mCherry adenoviruses, while the control
580 group was transduced with only cTnT-eGFP and/or cTnT-H2B-GFP and CMV-α-act-mCherry
581 adenoviruses. MOI of adenoviruses was adjusted to 180 in each well of the test (with cTnT-
582 hCCNA2; MOI 100, CMV-α-act-mCherry; MOI 40, and cTnT-eGFP or cTnT-H2B-GFP; MOI 40)
583 and the control (cTnT-eGFP; MOI 140 and CMV-α-act-mCherry; MOI 40) group. After 48 hours
584 of incubation, transduction was confirmed by observing the desired fluorescence in live cell
585 imaging with Zeiss AxioVision Observer Z1 inverted microscope (Carl Zeiss). We also tested the
586 differentiation potential (Ca^{2+} flux) of daughter cardiomyocytes after cytokinesis *in vitro* by
587 culturing them in an agarose-based semi-solid medium for 2 weeks. For calcium imaging, they
588 were seeded on a glass coverslip and grown in low serum (5% FBS without horse serum) and
589 0.5 mM calcium chloride for 10 days in a 3D matrix (agarose). For control cells (also daughter
590 cells post cytokinesis with CCNA2), 0.5 mM calcium chloride was not added. Cells were incubated
591 in Tyrode buffer containing 5μM Fluo3 dye for 30 minutes. Cells were washed with Tyrode buffer.
592 Cardiomyocytes were subjected to Ca^{2+} flux imaging with pacing of 0.5 Hz and 1 Hz current. The
593 flux was graphed as time (s) on the X-axis and Fluo3 intensity (Ca^{2+}) on the Y-axis.
594

595 **Time-lapse microscopy**

596 To capture cell division events in cardiomyocytes *in vitro*, we carried out live cell epifluorescence
597 time-lapse microscopy as described in [22]. In brief, Zeiss AxioVision Observer Z1 (Carl Zeiss,
598 Thornwood, NY, USA) inverted epifluorescence microscope in a humidified chamber in the
599 presence of 5% CO_2 at 37°C was used to carry out time-lapse microscopy. Multiple random
600 points with cells expressing eGFP (green) and mCherry (red) were selected in the test and control
601 groups. The positions were marked with the "position-list" tool in the AxioVision microscopy
602 software (AxioVision Release 4.7, Carl Zeiss). After the first cycle of imaging, only the channel for
603 Texas red was used (for detection of mCherry) to acquire images for 72 hours. The fluorescein
604 isothiocyanate (green) channel of the microscope was kept closed during the time-lapse imaging
605 to avoid cell death from exposure to ultraviolet rays in this channel. Images were taken at intervals
606 of 30 min. The 10X objective was used for all time-lapse imaging. Time-lapse movies were
607 generated after the end of each experiment and exported as MOV files. The time-lapse movies
608 were analyzed, and cells that underwent successful cytokinesis were enumerated in each group.
609 The percentage (%) of cytokinesis events was calculated for each position, and the graph was
610 plotted.
611
612

613 **Cell fixation and nuclear staining**
614 After time-lapse microscopy, cells in the glass-bottom plate were fixed with 4% paraformaldehyde
615 at room temperature for 20 min and were stored at 4°C. For nuclear staining, cells were washed
616 with 1x PBS then permeabilized with 0.5% Triton X-100 solution for 20 min at room temperature.
617 Cells were washed three times with 1x PBS and incubated in DAPI solution (2.5 µg/ml) for 5 min.
618 Cells were washed twice with 1x PBS, and imaging was carried out using a Zeiss AxioVision
619 Observer Z1 inverted epifluorescence microscope.
620
621 **Quantitative RT-PCR and Conventional PCR**
622 Quantitative PCR was performed in human adult cultured cardiomyocytes transduced with cTnT-
623 hCCNA2 (test) or cTnT-eGFP (control) adenoviruses with similar MOI (MOI 100). Reactions were
624 run on a StepOnePlus™ Real-Time PCR System (Applied Biosystems) using SYBR Green PCR
625 Master Mix (Applied Biosystems, Cat. #4309155). The PCR protocol consisted of: 95 °C for 2
626 min; 39 cycles of 95 °C for 15 s and 60 °C for 1 min; followed by melt-curve analysis. Gene
627 expression was quantified using the comparative Ct (ΔΔCt) method [22,57] with normalization to
628 *GAPDH*. A Ct value of 39 was assigned to reactions with a single detectable transcript. Fold
629 change was calculated as $2^{(39-\Delta\Delta Ct)}$, consistent with this detection threshold approach.

630 For mouse experiments, total RNA was isolated from CCNA2 transgenic (CCNA2-Tg), adult non-
631 transgenic (nTg) cardiomyocytes, and nTg postnatal day 2 (P2) hearts. RNA concentration was
632 determined using a Qubit 3.0 Fluorometer (Thermo Fisher Scientific). First-strand cDNA was
633 synthesized from total RNA using the High-Capacity cDNA Reverse Transcription Kit (Applied
634 Biosystems, Cat. #4368814) according to the manufacturer's instructions. Conventional PCR was
635 performed with mouse-specific primers for proliferation, cytokinesis, and reprogramming markers
636 **(Table S1)**, with *Gapdh* as the internal control. The PCR cycling conditions included: 95 °C for 10
637 min; 40 cycles of 95 °C for 30 s, 60 °C for 30 s, and 72 °C for 10 min; final hold at 4 °C. For
638 quantitative PCR, 10 ng cDNA was used per reaction with SYBR Green PCR Master Mix on the
639 StepOnePlus™ Real-Time PCR System. Data were normalized to endogenous control genes and
640 analyzed by the comparative Ct method as above [22,57]. Experiments were performed in triplicate.

641
642 **Animal**
643 Cyclin A2 transgenic mice, adult males, and females 8-12 weeks old (n=4), were maintained in a
644 B6CBA background [13, 19]. Non-transgenic (wild-type) littermates were used as controls (n=4).
645 Animals were housed in a temperature-controlled room with a 12:12 light/dark cycle and access
646 to water and food. All animal experiments were conducted in compliance with ARRIVE 2.0
647 guidelines. In selected experiments, animals received an intraperitoneal injection of heparin
648 (1000 U/mL; Sigma, H3393-50KU) to prevent coagulation during heart isolation for cardiomyocyte
649 isolation, and culture. Anesthesia was induced with isoflurane (Dechra) inhalation until loss of
650 pedal reflex confirmed deep anesthesia. While under deep anesthesia, mice were euthanized by
651 cervical dislocation, in accordance with the current AVMA guidelines, and all procedures were
652 performed to minimize pain and distress. A complete ARRIVE Essential 10 checklist is provided
653 in **Table S2**.
654

655 **Collection of CCNA2-Tg mouse hearts and sample preparation for single-nucleus**
656 **RNA-sequencing (snRNA-seq)**
657 Frozen heart tissues from CCNA2-Tg- and nTg adult mice, male and female, were minced and
658 transferred into a Dounce homogenizer containing ice-cold lysis buffer (Benthos Prime Central,
659 TX, USA). Samples were homogenized gently, and nuclei were isolated. Nuclei were ensured to
660 be free of clumps and debris by trypan blue staining under a microscope. Nuclei were then
661 counted, and the concentration was adjusted. 10x library concentration, insert size, and
662 quantification were checked using Qubit, Agilent bioanalyzer, and q-PCR, respectively. For data
663 Processing and Quality Control of 10x Sequencing of snRNA-seq, the reads were processed with
664 10X Genomics CellRanger software (v.3.1.0) with the default parameters for each sample. Cell
665 Ranger employs the STAR aligner for splicing-aware mapping of reads to the genome. It utilizes
666 a transcript annotation GTF file to categorize the reads into exonic, intronic, and intergenic regions
667 based on whether the reads align confidently with the genome. Only confidently mapped, non-
668 PCR duplicates with valid barcodes and UMIs were used to generate a gene-barcode matrix. This
669 involved various steps, including alignment to a reference, collapsing of unique molecular
670 identifiers (UMIs), UMI counting, and initial quality control procedures. The output of this process
671 was the generation of filtered gene expression matrices that exclusively contained cellular
672 barcodes. Subsequently, the Seurat R package (v.3.1.1) was used for data quality control and
673 downstream processing. The filtered_feature_bc_matrix generated by Cell Ranger was used for
674 Seurat processing. Post-sequencing quality control was performed using Seurat. Cells were
675 excluded from downstream processing in each sample if they met any of the following criteria:
676 fewer than 200 genes were detected per cell, genes had non-zero counts in at most three cells,
677 total feature counts exceeded 8000 (suggesting potential multiplets), more than 50% of the
678 feature count was attributable to mitochondrial genes, or more than 5% of the feature count was
679 attributable to hemoglobin-related genes, and doublets from all the clusters were filtered during
680 QC using DoubletFinder version 2.0.3 **(Figure S5)**. Raw read counts were log-normalized, cells
681 were clustered **(Figure S6)**, and markers for each cluster were identified by using the Seurat
682 FindMarkers and FindAllMarker functions [58]. The cell clusters were annotated by using the
683 iRhythmics FairdomHub instance (https://fairdomhub.org/studies/739) and prior knowledge.
684
685 **Human fetal and adult hearts and RNA sequencing**
686 Human fetal heart RNA (n=3 pooled, Cat #636532, Takara) and human adult heart RNA (n=4
687 pooled, Cat #636583, Takara) were used for bulk RNA sequencing with an increased read depth
688 (Ultra-deep sequencing), generating approximately 300 million reads per sample. This high
689 sequencing depth enabled the detection of rare transcripts, improved quantification accuracy, and
690 enhanced the resolution of transcript isoforms, including novel and unannotated RNAs. For library
691 preparation, we employed a ribosomal RNA (rRNA) depletion strategy instead of poly(A)
692 enrichment to capture both polyadenylated (polyA$^+$) and non-polyadenylated (polyA$^-$) RNAs.
693 While polyA$^+$ selection primarily enriches for mRNAs and some lncRNAs, rRNA depletion allows
694 for the inclusion of a broader spectrum of regulatory RNAs, including enhancer RNAs (eRNAs),
695 small nuclear RNAs (snRNAs), and uncharacterized lncRNAs that may lack poly(A) tails.
696 Additionally, this approach reduces transcript bias, preserves isoform diversity, and is better
697 suited for degraded RNA samples.

By combining rRNA depletion with ultra-deep sequencing, we achieved a comprehensive and unbiased profile of the cardiac transcriptome. The sequence reads were mapped to the human genome (GRCh38.110) using STAR [59] (version 2.7.9a). Using the mapped reads, the R package edgeR [60] (version 3.30.3) was employed to calculate counts per million (CPM) values and false discovery rate (FDR)-adjusted p-values obtained through the Benjamini–Hochberg method (Benthos Prime Central, TX, USA).

Comparative transcriptomic analysis of CCNA2-Tg and hypertrophic (TAB) cardiomyocytes

To delineate the transcriptional distinctions between regenerative and pathological remodeling, we compared CCNA2-Tg with cardiomyocytes from the murine transverse aortic banding (TAB) model (GSE138299) [37]. Bulk RNA-seq datasets were processed using counts per million (CPM), followed by geometric mean normalization based on validated, stably expressed housekeeping genes *(Rpl13a* and *Hprt1)*. This approach enabled a quantitative comparison of gene expression programs underlying CCNA2-driven regeneration versus stress-induced hypertrophic remodeling.

Pathway enrichment analysis

Pathway enrichment analysis was performed using the Reactome pathway analysis tool [61]. The differentially expressed genes among nTg and CCNA2-Tg conditions (log2FC > / < 1 and a P value < 0.05) were used for pathway analysis. Fold enrichment was calculated to indicate the gene expression observed in our list compared to the expected list. Categories with a fold enrichment greater than 1 were considered overrepresented, while those with a fold enrichment less than 1 were considered underrepresented in our experiment. Additionally, pathway enrichment analysis was conducted using BioPlanet via the EnrichR suite [62], following a previously described approach [63].

Statistical analysis

Statistical analyses were carried out using the R package (version 3.30.3), GraphPad Prism (version 8.2.1, GraphPad), and Python (via Google Colab). Two-tailed unpaired or paired *t*-tests were used for comparison between groups with normally distributed data. Chi-square (χ^2) tests for proportions were performed using Python libraries, including *Scipy*. The sample size (n) is reported for each analysis. Data are presented as means ± s.e.m unless otherwise indicated. Statistical significance was defined as $P < 0.05$. Effect sizes were computed using Cohen's d to assess the magnitude and directionality of expression changes between groups [64], defined as the difference between group means divided by the pooled standard deviation. The graph was generated in Python using Google Colab. We followed standard conventions for interpreting effect size magnitude: small (~0.2), medium (~0.5), and large (≥0.8). In this study, $|d| \geq 1.0$ was considered indicative of a strong effect.

Study approval

This study was conducted in accordance with the Declaration of Helsinki. Adult human cardiomyocytes were obtained from Anabios (San Diego, CA), which provides de-identified patient information as defined in the Health Insurance Portability and Accountability Act (HIPAA). Anabios consent procedures utilized meet the standard guidelines concerning informed consent

742 for research. For the mouse study, the protocol was approved by the Institutional Animal Care
743 and Use Committee (IACUC) of Mount Sinai Hospital, and all procedures adhered to the
744 Institutional Animal Care and Use Guidelines.
745
746 **Data availability**
747 The processed single-nucleus data and the deep bulk RNA sequencing, including raw expression
748 matrices and raw sequence files that support this research study's findings, are available on the
749 Gene Expression Omnibus GSE249433 and GSE256519, respectively. For comparative
750 analyses, publicly available transcriptomic data from hypertrophic hearts were obtained from
751 GSE138299 [37].
752

Abbreviations and Acronyms	
Actn2	Actinin Alpha 2
Atp2a2	ATPase, SERCA2
Atp5b	ATP Synthase, Mitochondrial F1 Complex, Beta Polypeptide ATP
Atp5g3	Synthase, Mitochondrial C Subunit, Gamma Polypeptide 3
Bub1	BUB1 Mitotic Checkpoint Serine/Threonine Kinase
C1qa	Complement C1q A Chain
Ca^{2+}	Calcium ion
Calm1	Calmodulin 1
Calm2	Calmodulin 2
CCNA2	Cyclin A2
CCNA2-Tg	CCNA2- transgenic mice
Cdc20	Cell Division Cycle 20
Cdk1	Cyclin-Dependent Kinase 1
Cdk2	Cyclin-Dependent Kinase 2
CGC	Cardiac glial cells
CMs	Cardiomyocytes
CPM	Counts per million
CTnT	Cardiac Troponin T
CTnT-hCCNA2	Cardiac Troponin T- human cyclin A2
E1/E2	Early region 1/Early region 2
EC	Endothelial cells
EC-derived FB	Endothelial-derived fibroblasts
EDC	Endocardial cells
Efnb2	Ephrin B2
eGFP	Enhanced Green Fluorescent Protein
EPC	Epicardial cells
EP-derived FB	Epicardial derived fibroblasts
ES	Embryonic stem cells
FB	Fibroblasts
FBS	Fetal Bovine Serum
FDR	False discovery rate
Gata4	GATA Binding Protein 4
H2B	Histone 2B
Igfbp3	Insulin-Like Growth Factor Binding Protein 3
iPS	Induced pluripotent
Kcnd2	Potassium Voltage-Gated Channel Subfamily D Member 2
Kif23	Kinesin Family Member 23
Klf4	Kruppel Like Factor 4
MI	Myocardial infarction
Mki67	Marker of Proliferation Ki-67
MOI	Multiplicity of Infection
Mono	Monocytes
Myc	MYC Proto-Oncogene, BHLH Transcription Factor
Myh7	Myosin Heavy Chain 7
Myl2	Myosin Light Chain 2
Myob	Myoblasts
NC	Neuronal cells
Neb	Nebulin
nTg	Non-transgenic mice
PEC	Pericytes

Pkp2	Plakophilin 2
Pln	Phospholamban
Pou5f1	POU Class 5 Homeobox 1, Oct4
Prc1	Protein Regulator of Cytokinesis 1
Pro-vCM	Proliferative ventricular cardiomyocyte
Ryr2	Ryanodine Receptor 2
Scn5a	Sodium Voltage-Gated Channel Alpha Subunit 5
SMC	Smooth muscle cells
SnRNA-seq	Single nucleus RNA sequencing
TC	T-Cells
Tnnc1	Troponin C1
Tnni3k	Troponin I Interacting Kinase
Top2a	Topoisomerase (DNA) II Alpha
t-SNE	T-distributed Stochastic Neighbor Embedding
Ttn	Titin
UMI	Unique molecular identifier
UnkC	Unknown cells
vCM	Ventricular cardiomyocyte
VEC	Vascular endothelial cells
α-act	Alpha-actinin

Acknowledgment

We thank Dr. Bernhard Kühn for his contribution to the cTnT-H2B-GFP utilized in this study. This work was supported by the National Institutes of Health National Heart, Lung, and Blood Institute (NIH R01 HL150345), the New York Stem Cell Science (NYSTEM C029565 and C32608GG).

Author Contributions

E.B. wrote the original article, contributed to experiments, and analyzed and performed snRNA-seq data with input from P.M. and A.K.; S.V.M and A.K.R contributed to cytokinesis experiments and calcium measurements; P.M. contributed to processing snRNA-seq samples and initial analysis; C.D.S. assisted with the cell biology experiments and organization of the manuscript; P.E.M., A.G., N.A.G. provided cardiomyocytes through their proprietary technology. H.W.C. was responsible for conceptualization, vector design, validation, supervision, reviewing, and funding acquisition. Review & editing- E.B, H.W.C, P.M., and A.K.

Competing interests

H.W.C. is the inventor of multiple patents regarding cyclin A2-mediated cardiac repair and caudal-related homeobox 2 cells for cardiac repair. She is in the midst of launching a new biotechnology company to advance such therapies to clinical development. Other authors declare no financial competing interests.

References

1 Yoshizumi, M. *et al.* Disappearance of cyclin A correlates with permanent withdrawal of cardiomyocytes from the cell cycle in human and rat hearts. *J Clin Invest* **95**, 2275-2280 (1995). https://doi.org/10.1172/JCI117918

2 Miyamoto, K. *et al.* Direct In Vivo Reprogramming with Sendai Virus Vectors Improves Cardiac Function after Myocardial Infarction. *Cell Stem Cell* **22**, 91-103 e105 (2018). https://doi.org/10.1016/j.stem.2017.11.010

3 Doppler, S. A. *et al.* Mammalian Heart Regeneration: The Race to the Finish Line. *Circ Res* **120**, 630-632 (2017). https://doi.org/10.1161/CIRCRESAHA.116.310051

4 Yoshida, Y. & Yamanaka, S. Induced Pluripotent Stem Cells 10 Years Later: For Cardiac Applications. *Circ Res* **120**, 1958-1968 (2017). https://doi.org/10.1161/CIRCRESAHA.117.311080

5 Shiba, Y. *et al.* Allogeneic transplantation of iPS cell-derived cardiomyocytes regenerates primate hearts. *Nature* **538**, 388-391 (2016). https://doi.org/10.1038/nature19815

6 Chong, J. J. *et al.* Human embryonic-stem-cell-derived cardiomyocytes regenerate non-human primate hearts. *Nature* **510**, 273-277 (2014). https://doi.org/10.1038/nature13233

7 Mollova, M. *et al.* Cardiomyocyte proliferation contributes to heart growth in young humans. *Proc Natl Acad Sci U S A* **110**, 1446-1451 (2013). https://doi.org/10.1073/pnas.1214608110

8 Bergmann, O. *et al.* Evidence for cardiomyocyte renewal in humans. *Science* **324**, 98-102 (2009). https://doi.org/10.1126/science.1164680

9 Brockes, J. P. & Kumar, A. Plasticity and reprogramming of differentiated cells in amphibian regeneration. *Nat Rev Mol Cell Biol* **3**, 566-574 (2002). https://doi.org/10.1038/nrm881

10 Poss, K. D., Wilson, L. G. & Keating, M. T. Heart regeneration in zebrafish. *Science* **298**, 2188-2190 (2002). https://doi.org/10.1126/science.1077857

11 Jopling, C. *et al.* Zebrafish heart regeneration occurs by cardiomyocyte dedifferentiation and proliferation. *Nature* **464**, 606-609 (2010). https://doi.org/10.1038/nature08899

12 Furtado, M. B., Nim, H. T., Boyd, S. E. & Rosenthal, N. A. View from the heart: cardiac fibroblasts in development, scarring and regeneration. *Development* **143**, 387-397 (2016). https://doi.org/10.1242/dev.120576

13 Chaudhry, H. W. *et al.* Cyclin A2 mediates cardiomyocyte mitosis in the postmitotic myocardium. *J Biol Chem* **279**, 35858-35866 (2004). https://doi.org/10.1074/jbc.M404975200

14 Nurse, P. A long twentieth century of the cell cycle and beyond. *Cell* **100**, 71-78 (2000). https://doi.org/10.1016/s0092-8674(00)81684-0

15 Pagano, M., Pepperkok, R., Verde, F., Ansorge, W. & Draetta, G. Cyclin A is required at two points in the human cell cycle. *EMBO J* **11**, 961-971 (1992). https://doi.org/10.1002/j.1460-2075.1992.tb05135.x

16 Sherr, C. J. & Roberts, J. M. Inhibitors of mammalian G1 cyclin-dependent kinases. *Genes Dev* **9**, 1149-1163 (1995). https://doi.org/10.1101/gad.9.10.1149

17 Wang, B. J. & Chaudhry, H. W. Regulation of Cardiomyocyte Division During Cardiac Regeneration. *Curr Cardiol Rep* **25**, 615-620 (2023). https://doi.org/10.1007/s11886-023-01886-7

18 Vadakke-Madathil, S. & Chaudhry, H. W. Cardiac Regeneration: Time to Revisit Nature. *Circ Res* **123**, 24-26 (2018). https://doi.org/10.1161/CIRCRESAHA.118.313246

19 Cheng, R. K. *et al.* Cyclin A2 induces cardiac regeneration after myocardial infarction and prevents heart failure. *Circ Res* **100**, 1741-1748 (2007). https://doi.org/10.1161/CIRCRESAHA.107.153544

20 Woo, Y. J. *et al.* Therapeutic delivery of cyclin A2 induces myocardial regeneration and enhances cardiac function in ischemic heart failure. *Circulation* **114**, I206-213 (2006). https://doi.org/10.1161/CIRCULATIONAHA.105.000455

21 Woo, Y. J. *et al.* Myocardial regeneration therapy for ischemic cardiomyopathy with cyclin A2. *J Thorac Cardiovasc Surg* **133**, 927-933 (2007). https://doi.org/10.1016/j.jtcvs.2006.07.057

22 Shapiro, S. D. *et al.* Cyclin A2 induces cardiac regeneration after myocardial infarction through cytokinesis of adult cardiomyocytes. *Sci Transl Med* **6**, 224ra227 (2014). https://doi.org/10.1126/scitranslmed.3007668

23 Litvinukova, M. *et al.* Cells of the adult human heart. *Nature* **588**, 466-472 (2020). https://doi.org/10.1038/s41586-020-2797-4

24 Bak, S. T. *et al.* Ploidy-stratified single cardiomyocyte transcriptomics map Zinc Finger E-Box Binding Homeobox 1 to underly cardiomyocyte proliferation before birth. *Basic Res Cardiol* **118**, 8 (2023). https://doi.org/10.1007/s00395-023-00979-2

25 So, J. *et al.* Robust single-nucleus RNA sequencing reveals depot-specific cell population dynamics in adipose tissue remodeling during obesity. *Elife* **13** (2025). https://doi.org/10.7554/eLife.97981

26 Galow, A. M. *et al.* Quality control in scRNA-Seq can discriminate pacemaker cells: the mtRNA bias. *Cell Mol Life Sci* **78**, 6585-6592 (2021). https://doi.org/10.1007/s00018-021-03916-5

27 Galow, A. M. *et al.* Integrative Cluster Analysis of Whole Hearts Reveals Proliferative Cardiomyocytes in Adult Mice. *Cells* **9** (2020). https://doi.org/10.3390/cells9051144

28 Lai, Z. F. *et al.* Overexpression of TNNI3K, a cardiac-specific MAP kinase, promotes P19CL6-derived cardiac myogenesis and prevents myocardial infarction-induced injury. *Am J Physiol Heart Circ Physiol* **295**, H708-716 (2008). https://doi.org/10.1152/ajpheart.00252.2008

29 Rajakumari, S. *et al.* EBF2 determines and maintains brown adipocyte identity. *Cell Metab* **17**, 562-574 (2013). https://doi.org/10.1016/j.cmet.2013.01.015

30 Wang, L. *et al.* Polymorphisms of the tumor suppressor gene LSAMP are associated with left main coronary artery disease. *Ann Hum Genet* **72**, 443-453 (2008). https://doi.org/10.1111/j.1469-1809.2008.00433.x

31 Liu, J. *et al.* Aberrantly high activation of a FoxM1-STMN1 axis contributes to progression and tumorigenesis in FoxM1-driven cancers. *Signal Transduct Target Ther* **6**, 42 (2021). https://doi.org/10.1038/s41392-020-00396-0

32 Zhao, L. *et al.* CD44 regulates vascular gene expression in a proatherogenic environment. *Arterioscler Thromb Vasc Biol* **27**, 886-892 (2007). https://doi.org/10.1161/01.ATV.0000259362.10882.c5

33 Beisaw, A. & Wu, C. C. Cardiomyocyte maturation and its reversal during cardiac regeneration. *Dev Dyn* **253**, 8-27 (2024). https://doi.org/10.1002/dvdy.557

34 Xing, Z. *et al.* Expression and prognostic value of CDK1, CCNA2, and CCNB1 gene clusters in human breast cancer. *J Int Med Res* **49**, 300060520980647 (2021). https://doi.org/10.1177/0300060520980647

35 Santamaria, D. *et al.* Cdk1 is sufficient to drive the mammalian cell cycle. *Nature* **448**, 811-815 (2007). https://doi.org/10.1038/nature06046

36 McLellan, M. A. *et al.* High-Resolution Transcriptomic Profiling of the Heart During Chronic Stress Reveals Cellular Drivers of Cardiac Fibrosis and Hypertrophy. *Circulation* **142**, 1448-1463 (2020). https://doi.org/10.1161/CIRCULATIONAHA.119.045115

37 Vigil-Garcia, M. *et al.* Gene expression profiling of hypertrophic cardiomyocytes identifies new players in pathological remodelling. *Cardiovasc Res* **117**, 1532-1545 (2021). https://doi.org/10.1093/cvr/cvaa233

38 Bersell, K., Arab, S., Haring, B. & Kuhn, B. Neuregulin1/ErbB4 signaling induces cardiomyocyte proliferation and repair of heart injury. *Cell* **138**, 257-270 (2009). https://doi.org/10.1016/j.cell.2009.04.060

39 Leeuwenburgh, B. P. *et al.* Chronic right ventricular pressure overload results in a hyperplastic rather than a hypertrophic myocardial response. *J Anat* **212**, 286-294 (2008). https://doi.org/10.1111/j.1469-7580.2008.00853.x

40 Assey, M. E., Wisenbaugh, T., Spann, J. F., Jr., Gillette, P. C. & Carabello, B. A. Unexpected persistence into adulthood of low wall stress in patients with congenital aortic stenosis: is there a fundamental difference in the hypertrophic response to a pressure overload present from birth? *Circulation* **75**, 973-979 (1987). https://doi.org/10.1161/01.cir.75.5.973

41 Torp, K. H. Congenital aortic stenosis with hyperplasia of the endocardium in the left ventricle. *Acta Pathol Microbiol Scand* **29**, 109-119 (1951). https://doi.org/10.1111/j.1699-0463.1951.tb00109.x

42 Kranenburg, O., van der Eb, A. J. & Zantema, A. Cyclin D1 is an essential mediator of apoptotic neuronal cell death. *EMBO J* **15**, 46-54 (1996).

43 Freeman, R. S., Estus, S. & Johnson, E. M., Jr. Analysis of cell cycle-related gene expression in postmitotic neurons: selective induction of Cyclin D1 during programmed cell death. *Neuron* **12**, 343-355 (1994). https://doi.org/10.1016/0896-6273(94)90276-3

44 Sofer-Levi, Y. & Resnitzky, D. Apoptosis induced by ectopic expression of cyclin D1 but not cyclin E. *Oncogene* **13**, 2431-2437 (1996).

45 Kong, G. *et al.* Functional analysis of cyclin D2 and p27(Kip1) in cyclin D2 transgenic mouse mammary gland during development. *Oncogene* **21**, 7214-7225 (2002). https://doi.org/10.1038/sj.onc.1205895

46 Liu, Y. & Kitsis, R. N. Induction of DNA synthesis and apoptosis in cardiac myocytes by E1A oncoprotein. *J Cell Biol* **133**, 325-334 (1996). https://doi.org/10.1083/jcb.133.2.325

47 Wang, J., Chenivesse, X., Henglein, B. & Brechot, C. Hepatitis B virus integration in a cyclin A gene in a hepatocellular carcinoma. *Nature* **343**, 555-557 (1990). https://doi.org/10.1038/343555a0

48 Bergmann, O. *et al.* Dynamics of Cell Generation and Turnover in the Human Heart. *Cell* **161**, 1566-1575 (2015). https://doi.org/10.1016/j.cell.2015.05.026

49 Soonpaa, M. H., Kim, K. K., Pajak, L., Franklin, M. & Field, L. J. Cardiomyocyte DNA synthesis and binucleation during murine development. *Am J Physiol* **271**, H2183-2189 (1996). https://doi.org/10.1152/ajpheart.1996.271.5.H2183

50 Gonzalez-Rosa, J. M. *et al.* Myocardial Polyploidization Creates a Barrier to Heart Regeneration in Zebrafish. *Dev Cell* **44**, 433-446 e437 (2018). https://doi.org/10.1016/j.devcel.2018.01.021

51 Botting, K. J. *et al.* Early origins of heart disease: low birth weight and determinants of cardiomyocyte endowment. *Clin Exp Pharmacol Physiol* **39**, 814-823 (2012). https://doi.org/10.1111/j.1440-1681.2011.05649.x

52 Patergnani, S. *et al.* Various Aspects of Calcium Signaling in the Regulation of Apoptosis, Autophagy, Cell Proliferation, and Cancer. *Int J Mol Sci* **21** (2020). https://doi.org/10.3390/ijms21218323

53 Rosendo-Pineda, M. J., Moreno, C. M. & Vaca, L. Role of ion channels during cell division. *Cell Calcium* **91**, 102258 (2020). https://doi.org/10.1016/j.ceca.2020.102258

54 Liu, C. *et al.* Alteration of calcium signalling in cardiomyocyte induced by simulated microgravity and hypergravity. *Cell Prolif* **53**, e12783 (2020). https://doi.org/10.1111/cpr.12783

55 Bode, D., Cull, A. H., Rubio-Lara, J. A. & Kent, D. G. Exploiting Single-Cell Tools in Gene and Cell Therapy. *Front Immunol* **12**, 702636 (2021). https://doi.org/10.3389/fimmu.2021.702636

56 Yu, P. *et al.* Transcriptome Analysis of Hypertrophic Heart Tissues from Murine Transverse Aortic Constriction and Human Aortic Stenosis Reveals Key Genes and Transcription Factors Involved in Cardiac Remodeling Induced by Mechanical Stress. *Dis Markers* **2019**, 5058313 (2019). https://doi.org/10.1155/2019/5058313

57 Pfaffl, M. W. A new mathematical model for relative quantification in real-time RT-PCR. *Nucleic Acids Res* **29**, e45 (2001). https://doi.org/10.1093/nar/29.9.e45

58 Koenig, A. L. *et al.* Single-cell transcriptomics reveals cell-type-specific diversification in human heart failure. *Nat Cardiovasc Res* **1**, 263-280 (2022). https://doi.org/10.1038/s44161-022-00028-6

59 Dobin, A. *et al.* STAR: ultrafast universal RNA-seq aligner. *Bioinformatics* **29**, 15-21 (2013). https://doi.org/10.1093/bioinformatics/bts635

60 Robinson, M. D., McCarthy, D. J. & Smyth, G. K. edgeR: a Bioconductor package for differential expression analysis of digital gene expression data. *Bioinformatics* **26**, 139-140 (2010). https://doi.org/10.1093/bioinformatics/btp616

61 Fabregat, A. *et al.* Reactome pathway analysis: a high-performance in-memory approach. *BMC Bioinformatics* **18**, 142 (2017). https://doi.org/10.1186/s12859-017-1559-2

62 Xie, Z. *et al.* Gene Set Knowledge Discovery with Enrichr. *Curr Protoc* **1**, e90 (2021). https://doi.org/10.1002/cpz1.90

63 Huang, R. *et al.* The NCATS BioPlanet - An Integrated Platform for Exploring the Universe of Cellular Signaling Pathways for Toxicology, Systems Biology, and Chemical Genomics. *Front Pharmacol* **10**, 445 (2019). https://doi.org/10.3389/fphar.2019.00445

64 Cohen, J. *Statistical power analysis for the behavioral sciences*. 2nd edn, (L. Erlbaum Associates, 1988).

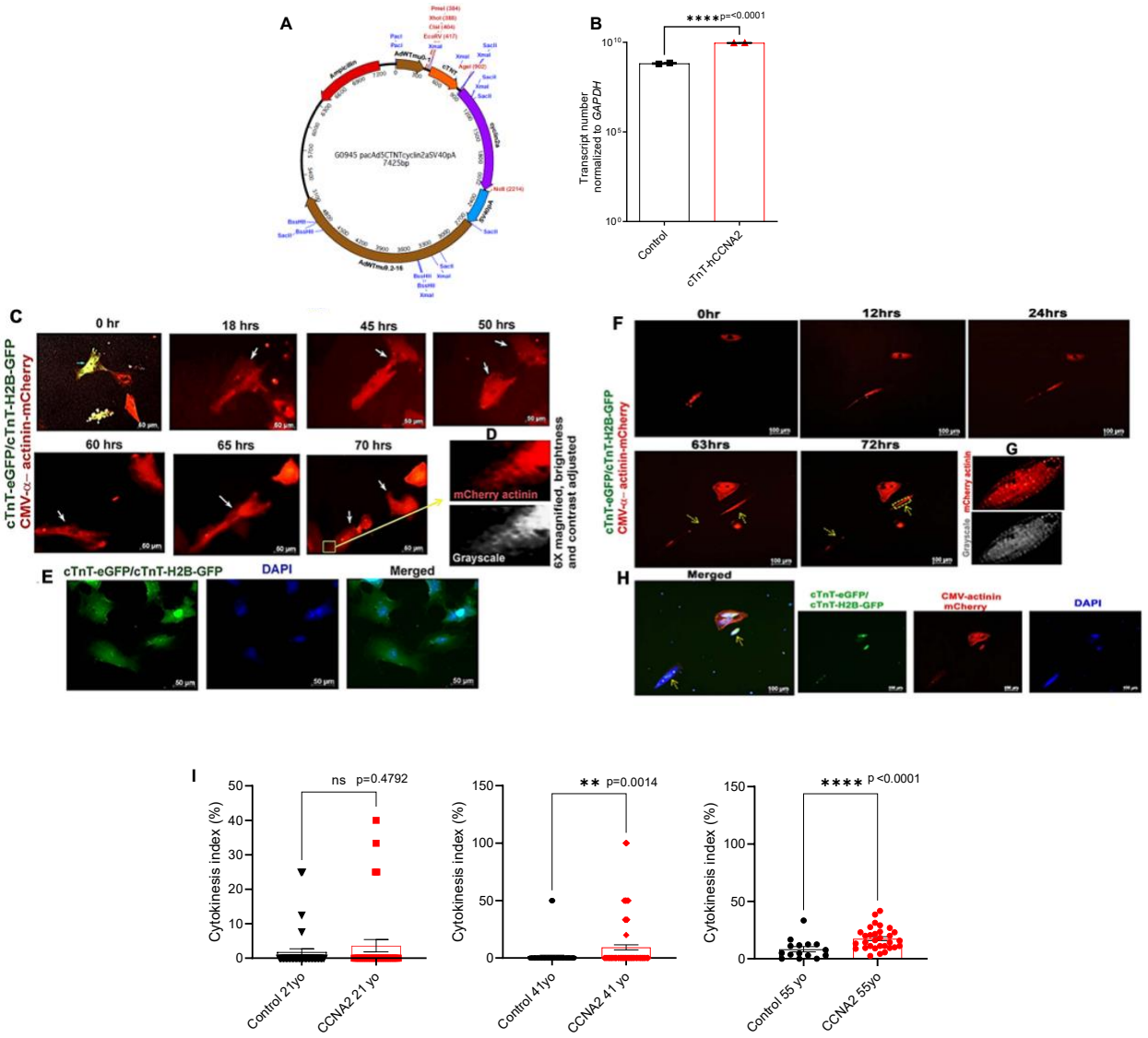

Figure 1. CCNA2 expression induces cytokinesis in adult human cardiomyocytes *In Vitro*. **A)** Clinical-use grade replication-deficient human adenovirus type 5 (Ad5) was used for this study. The vector was designed with cardiac Troponin T (cTnT) promoter to express human cyclin A2 (hCCNA2) specifically in cardiomyocytes. **B)** The cTnT-hCCNA2 adenovirus was used to transduce cultured adult human cardiomyocytes to induce the expression of CCNA2. Significantly higher CCNA2 expression was observed in cells transduced with cTnT-hCCNA2 compared to the control virus. **C-H)** From **Movies S1** and **S2**: still images from representative time-lapse epifluorescence microscopy of cultured cardiomyocytes isolated from adult humans **C**) 55-year-old and **F)** 41-year-old. Please note that still images of 55 and 41-years-old have scale bars of 50µm and 100µm as it is shown in the Movies S1 and S2 respectively. Cells were transduced with cTnT-hCCNA2, cTnT-H2B-GFP, cTnT-eGFP (to label cardiomyocytes), and CMV-α-actinin-m-Cherry adenoviruses prior to the beginning of the time-lapse imaging. **C)** At time 0 hr, a cell (yellow) expressing both cTnT (green) and α-actinin (red) was followed for 70 hrs via time-lapse microscopy. The green channel was closed, and cells were only followed through the red channel to avoid UV photo-toxicity. The observed human cardiomyocytes show the 1st cell division at 50 hrs of imaging, and one of the daughter cells subsequently undergoes division at 70 hrs of

969 imaging. **D** and **G)** At 70/72 hrs, a daughter cell is partially magnified with a grayscale version to
970 demonstrate the presence of an intact sarcomere structure. **E, H)** 1 day after live imaging ended,
971 these wells were fixed with subsequent labeling of nuclei with DAPI. The green fluorescence of
972 the original cTnT-eGFP and cTnT-H2B-GFP transduction is visible, further confirming that these
973 cells are cardiomyocytes. **I)** The cytokinetic events were counted in the control and test samples
974 from the 21-, 41-, and 55-year-old subjects. A significantly higher rate of cytokinesis was observed
975 in the test samples from the 41-year-old (p=0.001) and 55-year-old (p<0.0001) compared to the
976 control. On the other hand, the control and test samples from the 21-year-old did not exhibit a
977 significant difference in cytokinetic events (p=0.47). Data are represented as mean ± s.e.m.
978

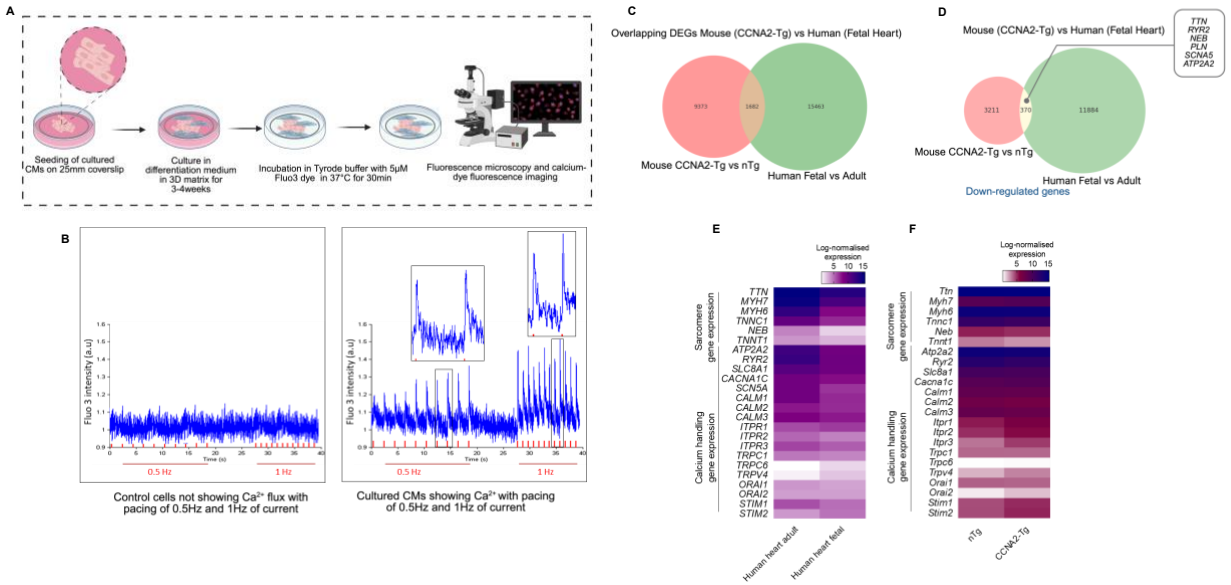

Figure 2. Differentiation of cultured adult human cardiomyocytes. Cultured adult human cardiomyocytes typically undergo dedifferentiation and were then subjected to 3D redifferentiation culture conditions and examined for Ca^{2+} flux. **A)** Overview of the 3D culture method of differentiation, Ca^{2+} flux measurement, and fluorescence microscopy in adult human cardiomyocytes. **B)** Representative Ca^{2+} flux graphs of re-differentiated cultured adult human cardiomyocytes. Ad5-cTnT-hCCNA2 transduced adult human cardiomyocytes treated with differentiation medium show Ca^{2+} flux with pacing of 0.5 and 1 Hz of current, while low Ca^{2+} flux was detected in the non-treated Ad5-cTnT-hCCNA2 transduced cardiomyocytes. **C)** Venn diagram showing the overlap of differentially expressed genes between CCNA2-Tg versus non-nTg mouse cardiomyocytes and human fetal versus adult hearts. **D)** Venn diagram displaying the subset of downregulated genes shared between the CCNA2-Tg mouse hearts and the fetal human heart. These genes include several associated with cardiomyocyte maturation. **E)** Heatmap depicting the expression of Ca^{2+} handling, contractility, and sarcomere-associated genes in human adult versus fetal hearts, **F)** Comparison of gene expression in cardiomyocytes from CCNA2-Tg versus nTg mice, highlighting differences in Ca^{2+} regulatory genes and contractile machinery. Positive values indicate upregulation in adult hearts relative to fetal hearts. Data represent normalized RNA-sequencing expression values. The illustration in (**A**) was created using BioRender (https://biorender.com).

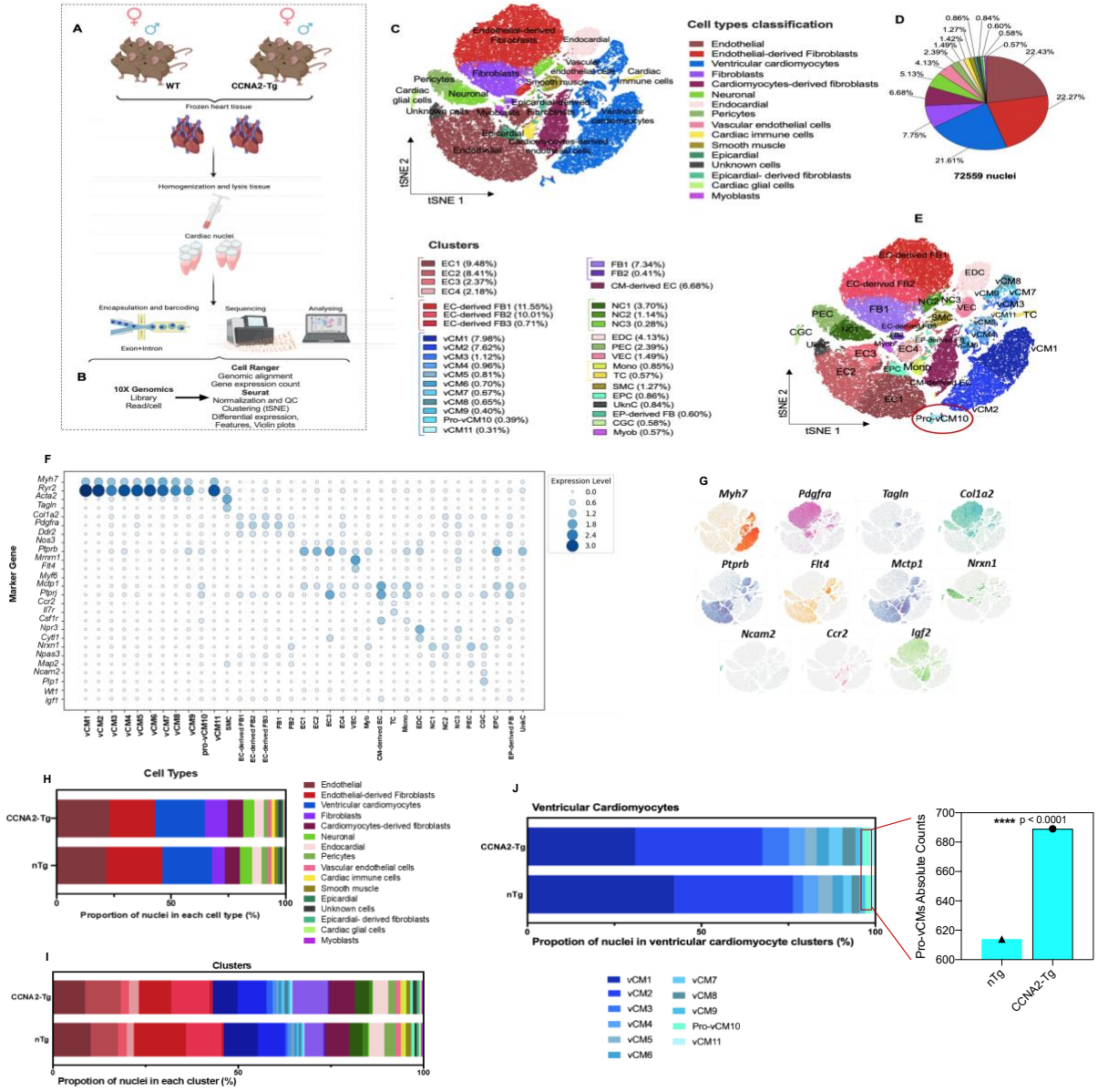

Figure 3. Single-nucleus RNA sequencing identified major cell types in CCNA2-Tg mice
A) Schematic depicting the design of the snRNA-seq experiments (n=2) for each condition nTg female, CCNA2-Tg female, nTg male, and nTg male. (*n*= 8 mice in total). **B)** The analysis pipeline and single-cell barcoded library generation (10X Genomics), sequence alignment (Cell Ranger), and further analysis using R (SeuratR package). (*n*= total nuclei 72,559) **C)** t-distributed Stochastic Neighbor Embedding (t-SNE) clustering the nuclei reveals more than 16 distinct major cell types identified based on the cell-specific markers dataset provided at iRhythmics FairdomHub instance, and **D)** the pie chart showing the proportion of cells within the snRNA-seq. **E)** t-SNE of a total of 35 subclusters. **F)** Dot plot depicting the expression levels of some of the key marker genes used to classify cell types. Dot size represents the percentage of cells expressing each gene, while color intensity reflects expression levels. **G)** Feature plots highlighting the expression of selected cell-type-specific markers across the t-SNE space. **H)** Stacked bar plots representing the proportion of nuclei classified into each major cell type (top) and **I)** each identified cluster (bottom) in both CCNA2-Tg and nTg mice. **J)** Stacked bar plots

1017 displaying the proportion of nuclei in vCM clusters (left). The absolute count comparison (right)
1018 highlights a significant increase in Pro-vCM10 in CCNA2-Tg hearts relative to nTg controls
1019 (****p<0.0001, Chi-square test), supporting the role of CCNA2 in promoting cardiomyocyte
1020 proliferation. CM: Cardiomyocytes, vCM: ventricular cardiomyocytes, EC: endothelial cells, FB:
1021 fibroblasts, EC-derived FB: endothelial-derived fibroblasts, NC: neuronal, EDC: endocardial cells.
1022 PEC: pericytes, VEC: vascular endothelial cells, Mono: monocytes, TC: T-Cells, SMC: smooth
1023 muscle cells, EPC: epicardial cells, UnkC: unknown cells, EP-derived FB: epicardial-derived
1024 fibroblasts, CGC: Cardiac glial cells, Myob: myoblasts. The illustration in (**A**) was created using
1025 BioRender (https://biorender.com).

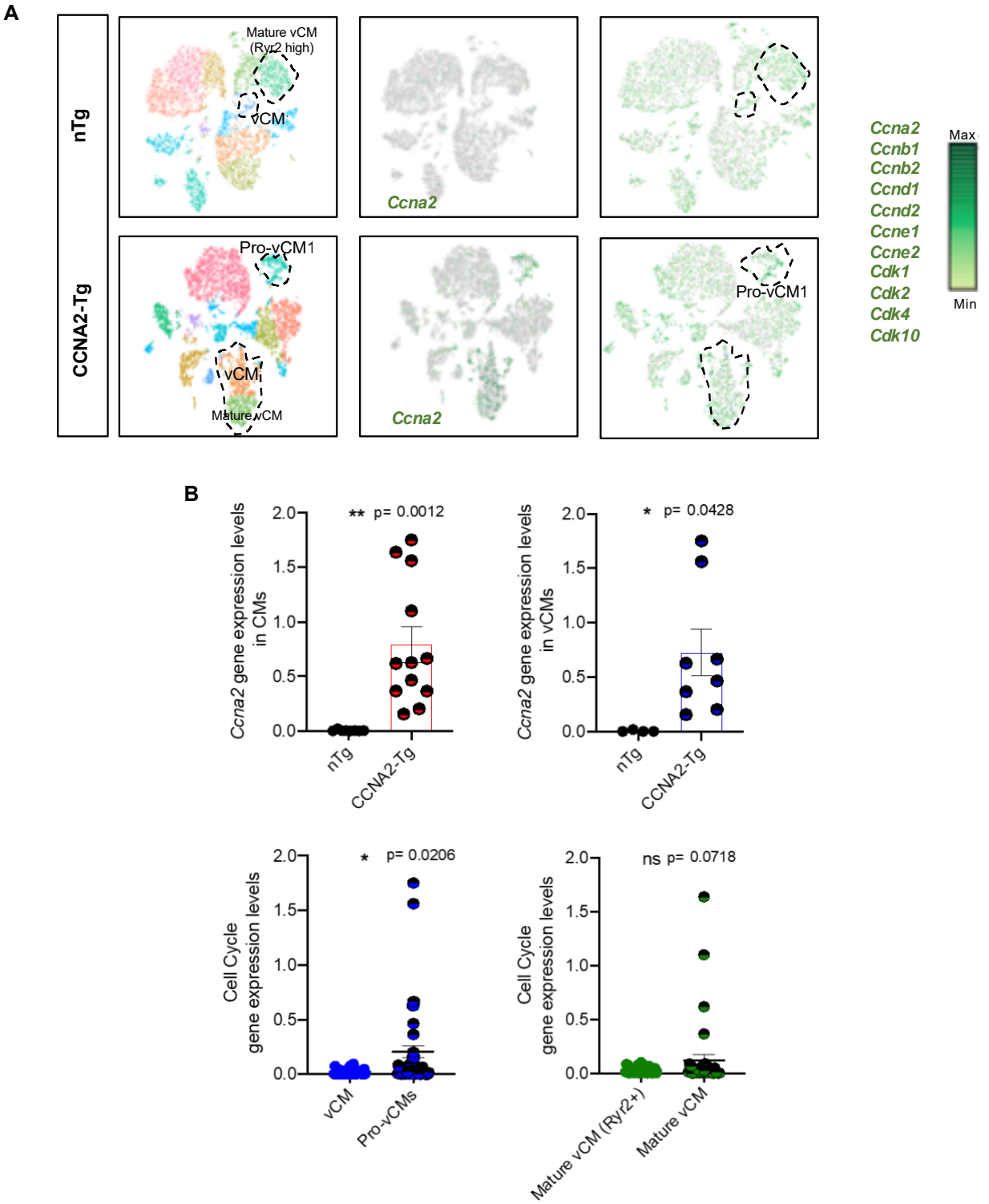

Figure 4. CCNA2 and cell cycle genes expression in CCNA2-Tg and nTg mice cardiomyocytes delineated by snRNA-seq. A) CCNA2 was expressed in the vCM, specifically

1029 in the pro-vCM subset of the cardiomyocyte population in CCNA2-Tg, and cell cycle genes
1030 projected on the t-SNE plot. **B)** Scatter plots showing the expression level of CCNA2 and cell
1031 cycle genes in cardiomyocytes of CCNA2-Tg and nTg mice. Each point represents an individual
1032 value; the mean value is represented by the horizontal line. Error bars represent s.e.m.

1033

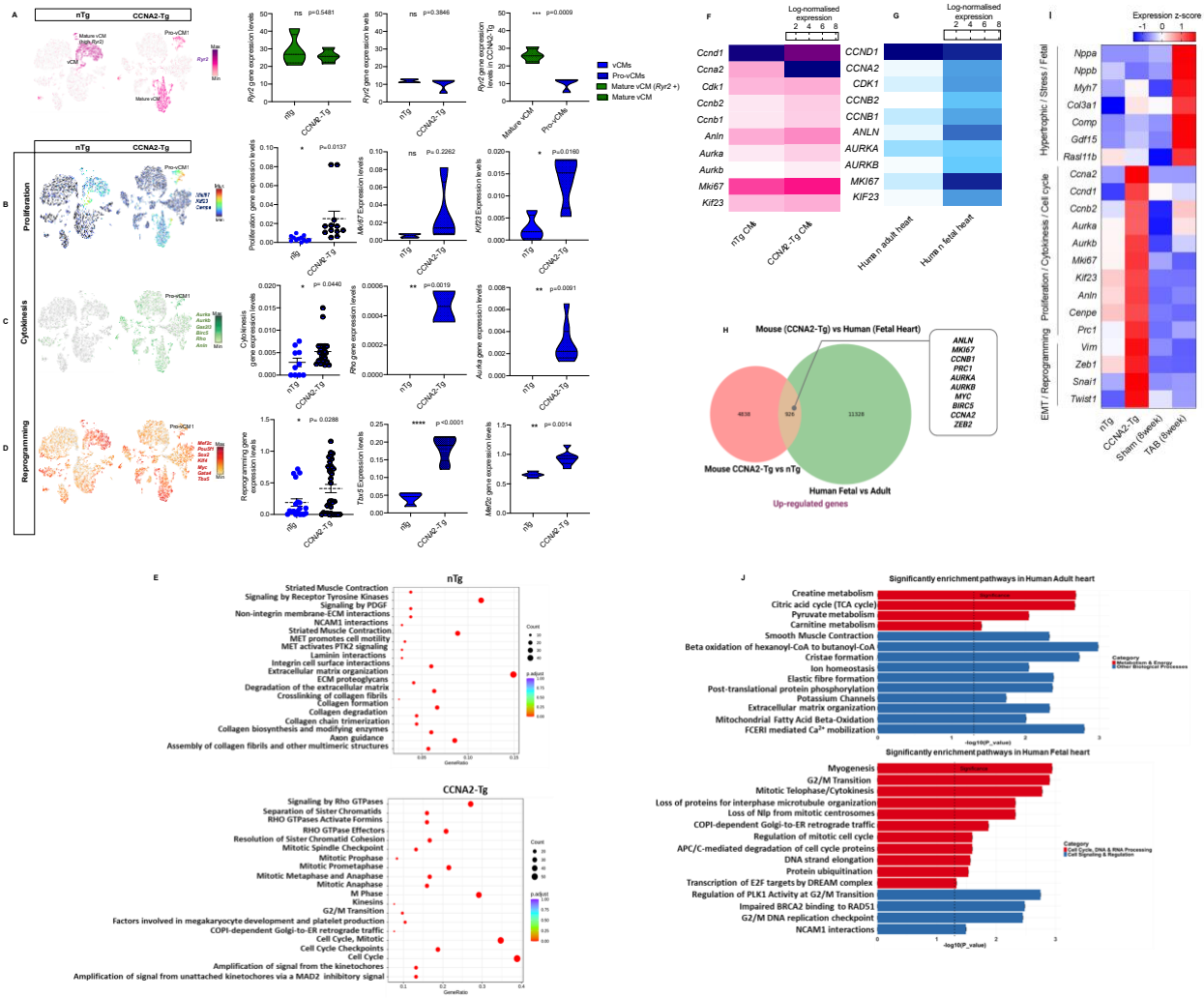

Figure 5. CCNA2 expression induces reprogramming, cytokinesis, and proliferation in mouse cardiomyocytes. A) t-SNE projection showing *Ryr2* expression across cardiomyocyte subpopulations in nTg and CCNA2-Tg mice. *Ryr2*+ cardiomyocytes correspond to a more mature ventricular cardiomyocyte (vCM) state, whereas *Ryr2* low-expression cardiomyocytes represent less mature, or proliferative cardiomyocytes. Quantification of *Ryr2* expression levels among cardiomyocyte subpopulations is shown in the accompanying violin plot, highlighting differences in *Ryr2* expression across conditions. **B)** t-SNE plots and representative scatter plots and Violin plots representing the expression of key proliferation, **C)** cytokinesis, and **D)** reprogramming gene markers in both CCNA2-Tg and nTg mice. Individual points represent median-normalized expression values for proliferation genes in Pro-vCMs. Two values were flagged as statistical outliers; these are retained to reflect biological heterogeneity within the proliferative program. **E)** Representative dot plot of the differential gene expression analysis showing the upregulation of proliferation, cytokinesis, and reprogramming genes in CCNA2-Tg versus nTg cardiomyocytes. **F)** Heatmaps of log-transformed gene expression changes in human fetal versus adult hearts, **G)** and in CCNA2-Tg versus nTg cardiomyocytes. **H)** Venn diagram showing shared upregulated genes between CCNA2-transgenic mouse hearts and human fetal hearts. The diagram displays the overlap of upregulated genes from CCNA2-Tg versus nTg mouse cardiomyocytes and human fetal versus adult heart RNA-seq datasets. These shared genes are further associated with cell cycle, cytokinesis, and cardiac development, supporting a dedifferentiation and reprogramming

1055 phenotype induced by CCNA2. **I)** Heatmap showing expression z-scores of canonical
1056 hypertrophic markers alongside genes associated with EMT and cell cycle /cytokinesis across
1057 different conditions: non-transgenic nTg, CCNA2-Tg, Sham-operated, and (8 weeks) transverse
1058 aortic banding (TAB) cardiomyocytes. The heatmap illustrates distinct gene expression patterns
1059 differentiating CCNA2-induced regenerative reprogramming from hypertrophic remodeling in
1060 pathological pressure overload. **J)** Pathway enrichment analysis showing significantly enriched
1061 pathways in the human adult (top) and fetal (bottom) heart. In the adult heart, pathways related
1062 to metabolism and energy are enriched, based on 4,348 downregulated genes and 3,713
1063 upregulated genes ($P<0.05$). In the fetal heart, cell cycle, DNA/RNA processing, and signaling
1064 pathways are enriched ($P<0.05$).

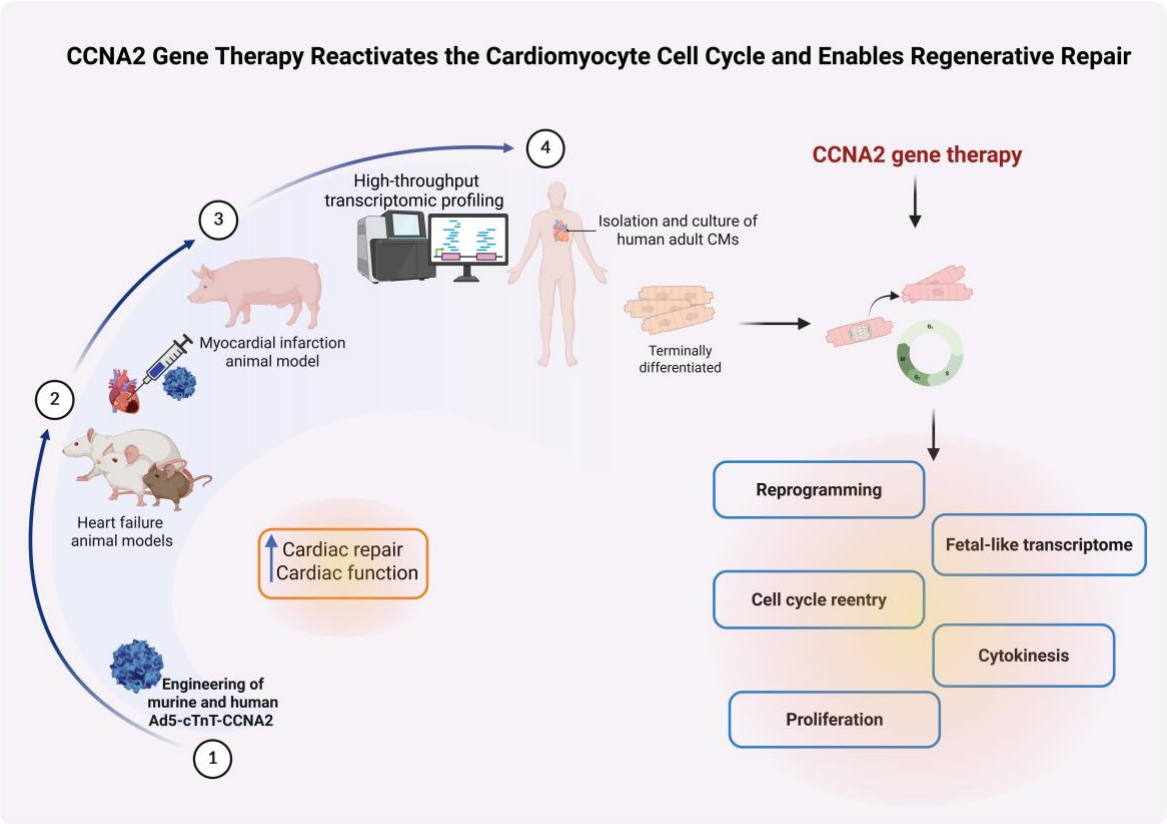

Figure 6. Translational roadmap and mechanistic model of CCNA2 gene therapy for cardiac regeneration. Building upon our previous *in vivo* studies in rodent and porcine myocardial infarction models, which demonstrated functional recovery via CCNA2 gene therapy (1-3) [13,19-22], this study provides direct evidence of complete cytokinesis in cultured human adult cardiomyocytes. Complementary transcriptomic analyses from fetal and adult human hearts, as well as CCNA2 transgenic models, reveal reactivation of reprogramming, fetal-like, and proliferative gene programs. The schematic illustrates the translational trajectory from preclinical to mechanistic insights and highlights CCNA2 as a driver of cardiomyocyte cell cycle reentry, cytokinesis, and regenerative gene expression. The illustration was created using BioRender (https://biorender.com).